國 立 交 通 大 學

電信工程學系

博 士 論 文

具頻率相關耦合之步階阻抗諧振器的準橢圓函數
響應濾波器之合成與實現

Synthesis and Realization of Frequency-Dependent
Coupled Stepped-Impedance Resonator Filters with a
Quasi-Elliptic Function Response

研 究 生： 徐慶陸 （Ching-Luh Hsu）

指導教授： 郭仁財 博士 （Dr. Jen-Tsai Kuo）

中 華 民 國 九十七 年 七 月

具頻率相關耦合之步階阻抗諧振器的準橢圓函數響應濾波器之合成與實現

Synthesis and Realization of Frequency-Dependent Coupled Stepped-Impedance Resonator Filters with a Quasi-Elliptic Function Response

研究生：徐慶陸　　　　　　　　　　Student: Ching-Luh Hsu

指導教授：郭仁財　博士　　　　　　Advisor: Dr. Jen-Tsai Kuo

國 立 交 通 大 學

電 信 工 程 學 系

博 士 論 文

A Dissertation
Submitted to Institute of Communication Engineering
College of Electrical and Computer Engineering
National Chiao Tung University
in Partial Fulfillment of the Requirements
for the Degree of Doctor of Philosophy
in
Communication Engineering
July 2008
Hsinchu, Taiwan

中 華 民 國 九 十 七 年 七 月

推　薦　函

一、　事由：本校電信研究所博士班研究生　徐慶陸　提出論文以參加

　　　國立交通大學博士班論文口試。

二、　說明：本校電信研究所博士班研究生　徐慶陸　已完成本校電信

　　　研究所規定之學科課程及論文研究之訓練。
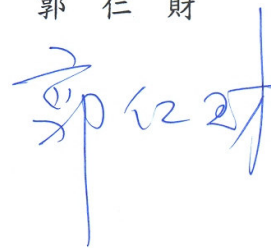
　　　有關學科部分，徐君已修滿十八學分之規定（請查閱學籍資料）

　　　並通過資格考試。

　　　有關論文部分，徐君已完成其論文初稿，相關之論文亦分別發

　　　表或即將發表於國際期刊（請查閱附件）並滿足論文計點之要

　　　求。

　　　總而言之，徐君已具備國立交通大學電信研究所應有之教育及

　　　訓練水準，因此特推薦

　　　徐君參加國立交通大學電信工程學系博士班論文口試。

交通大學電信工程學系教授　　郭　仁　財

國 立 交 通 大 學

論 文 口 試 委 員 審 定 書

本校 電 信 工 程 學系博士班 徐 慶 陸 君

所提論文 具頻率相關耦合之步階阻抗諧振器的準橢圓函數響應
濾波器之合成與實現

Synthesis and Realization of Frequency-Dependent Coupled
Stepped-Impedance Resonator Filters With a Quasi-Elliptic
Function Response

合於博士資格水準、業經本委員會評審認可。

口試委員: _____ _____

_____ _____

_____ _____

_____ _____

指導教授: _____ _____

系 主 任: _____ 教授

中 華 民 國 九 十 七 年 七 月 十 七 日

Department of Communication Engineering
National Chiao Tung University
Hsinchu, Taiwan, R.O.C.

Date: **July 17, 2008**

We have carefully read the dissertation entitled

Synthesis and Realization of Frequency-Dependent Coupled

Stepped-Impedance Resonator Filters With a Quasi-Elliptic Function

Response

submitted by _____**Ching-Luh Hsu**_____ in partial

fulfillment of the requirements of the degree of DOCTOR OF

PHILOSOPHY and recommend its acceptance.

Thesis Advisor: _____

Chairman
Department of Communication Engineering: _____

具頻率相關耦合之步階阻抗諧振器的準橢圓函數響應濾波器之合成與實現

研究生: 徐慶陸　　　　　　　　　指導教授: 郭仁財 博士

國立交通大學

電信工程學系

摘要

本論文研究具頻率相關耦合結構的濾波器合成與實現。首先探討具頻率相關耦合特性的三元結構(Trisection)，產生一對傳輸零點的機制。具有此類型零點的濾波器一般稱為準橢圓濾波器。僅使用頻率無關耦合特性的三元結構，通常只能產生一個傳輸零點。本文所提出的新型三元結構能產生一對零點。濾波器合成的演算過程中，頻率相關耦合結構的電路模型是將複數頻率變數 s 乘以固定導納轉換器(J-inverter)。研究發現分接線(Tapped-line)結構的輸入輸出會產生更多零點。文中將呈現具四個零點的三階電路以及具五個零點的四階電路設計。論文的第二部分探討平行緊密並排的步階阻抗諧振濾波器。研究發現此結構的非相鄰諧振器之間亦具有頻率相關的耦合特性。因此，濾波器的通帶兩側也會各產生一個零點，使過渡帶具有較大的衰減斜率。除此之外，分接線輸入輸出結構所產生的零點也會加以探究。文中所有電路的模擬結果和測量數據都相當一致。

Synthesis and Realization of Frequency-Dependent Coupled Stepped-Impedance Resonator Filters with a Quasi-Elliptic Function Response

Student: Ching-Luh Hsu   Advisor: Dr. Jen-Tsai Kuo

Department of Communication Engineering

National Chiao Tung University

Abstract

This dissertation aims at synthesis and realization of microstrip coupled- resonator filters with frequency-dependent cross-coupling. The first part presents the synthesis of trisection filters incorporating the frequency-dependent coupling to achieve a quasi-elliptic function response. In the admittance matrix of the lowpass prototype, the coupling is simply modeled by a constant J-inverter multiplied by the complex frequency variable s. In realization, tapped-line input/output is used and more zeros can be generated in the upper and lower rejection bands. The second part studies stepped-impedance resonators in a compact inline arrangement. It is found that certain transmission zeros can be created by nonadjacent frequency-dependent coupling. Enhanced attenuation rate of transition can then be obtained. Zeros created by tapped input/output structure are also investigated. For demonstrations, measured results for experimental filters are compared with simulation data.
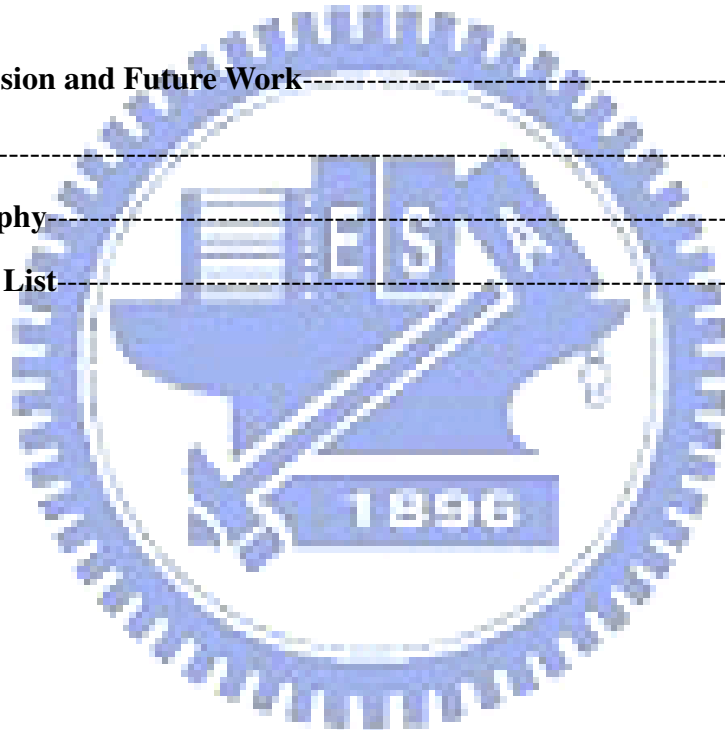
Contents

List of Figures

V

CHAPTER 1

Introduction

High-performance bandpass filters with low loss, high selectivity, linear phase, compact size, and wide stopband are essential to design of the RF front-ends for modern wireless/microwave communication systems. For microwave coupled-resonator filters, frequency selectivity and phase responses are related to the arrangement of resonators, source, and load. Extensive research has been drawn to this study for decades. A survey of the major development can be found in [1-11].

It is well-known that coupled-resonators in a sequence can be only used to realize the filters with a maximally-flat or equal-ripple response [12]. If a number of routes can be arranged between the input and output terminations in the filter, the sum of the transmitted signals through different routes may vanish on the output port at certain frequencies. Therefore, transmission zeros can be generated at these frequencies and the rejection level of the stopband can be then improved. For example, a single transmission zero can be produced in a three-resonator filter if the first resonator is simultaneously coupled to the second and the third resonators [13]. The zero can be placed in either the upper or the lower rejection band depending on the phase relationship of the signals through different routes. A second well-known example is the quadruplet, which has a pair of transmission zeros on each side of the passband. Coaxial resonators [14] and circular cavities [15] are proposed to realize this configuration by bridging the first and the fourth resonating elements with negative cross-coupling, respectively. It is worth pointing out that there are four resonators in the equivalent circuit of the filter in [15] although there are only two

physical cavities. In fact, each circular cavity is a dual-mode resonator. This dual-mode cavity filter has several advantages including lower loss, reduced weight, and multiple transmission zeros. Eventually, filters of this type become a standard in satellite communication industry [16]. In [17-18], it is revealed that the in-band phase can be equalized if the pair of zeros is placed on the real axis in the complex frequency plane. For obtaining such zeros, positive cross-coupling must be established between the first and the fourth resonators.

Many complex structures for coupled-resonator filters have been proposed to achieve more stringent responses. Nowadays, applications can be found in virtually any type of microwave communication systems including satellite, terrestrial, and mobile communications. In section 1.1, the structures suitable for microwave coupled-resonator filters are briefly surveyed. The motivation and the contribution of this research are addressed in section 1.2 and 1.3, respectively. Finally, the outline of the dissertation is given in section 1.4.

1.1 The Structures of Coupled-Resonator Filters

Generally speaking, a lumped-element equivalent circuit can be used to model a coupled-resonator filter. Fig. 1.1 shows the equivalent circuit of a direct-coupled waveguide filter with N cavities [12]. Each mutual inductive coupling is used to model an iris on the conductive wall between cavities. It is noted that only adjacent resonators are mutually coupled. Filter based on this structure can have a maximally-flat or Chebyshev response, i.e. an all-pole response, since there is no finite transmission zero in the $|S_{21}|$ response. The impedance matrix of the equivalent circuit can be easily derived and expressed as
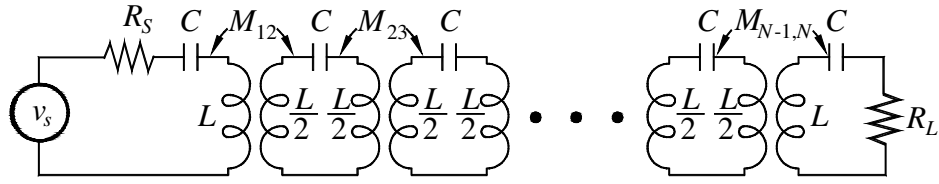
Fig. 1.1. The equivalent circuit of a direct-coupled waveguide filter with an all-pole response.

$$\begin{bmatrix} v_s \\ 0 \\ 0 \\ . \\ . \\ 0 \\ 0 \end{bmatrix} = \begin{bmatrix} R_S + j\Omega & j\omega M_{12} & 0 & . & . & 0 & 0 \\ j\omega M_{12} & j\Omega & j\omega M_{23} & . & . & 0 & 0 \\ 0 & j\omega M_{23} & j\Omega & . & . & 0 & 0 \\ . & . & . & . & . & . & . \\ . & . & . & . & . & . & . \\ 0 & 0 & 0 & . & . & j\Omega & j\omega M_{N-1,N} \\ 0 & 0 & 0 & . & . & j\omega M_{N-1,N} & R_L + j\Omega \end{bmatrix} \begin{bmatrix} i_1 \\ i_2 \\ i_3 \\ . \\ . \\ i_{N-1} \\ i_N \end{bmatrix} \quad (1.1.1)$$

where i_1, i_2, i_3, and i_4 are the loop currents, $\Omega = \sqrt{\dfrac{L}{C}}\left(\dfrac{\omega}{\omega_0} - \dfrac{\omega_0}{\omega}\right)$, $\omega_0 = 1/\sqrt{LC}$. For

narrow-band applications, it is noted that $\omega M_{i,j}$ can be approximately by $\omega_0 M_{i,j}$ [12].

Equation (1.1.1) can be then expressed as

$$\begin{bmatrix} v_s \\ 0 \\ 0 \\ . \\ . \\ 0 \\ 0 \end{bmatrix} = \begin{bmatrix} g_0 + jg_1\Omega & j & 0 & . & . & 0 & 0 \\ j & jg_2\Omega & j & . & . & 0 & 0 \\ 0 & j & jg_3\Omega & . & . & 0 & 0 \\ . & . & . & . & . & . & . \\ . & . & . & . & . & . & . \\ 0 & 0 & 0 & . & . & jg_{N-1}\Omega & j \\ 0 & 0 & 0 & . & . & j & g_{N+1} + jg_N\Omega \end{bmatrix} \begin{bmatrix} i_1 \\ i_2 \\ i_3 \\ . \\ . \\ i_{N-1} \\ i_N \end{bmatrix} \quad (1.1.2)$$

The equivalence of (1.1.1) and (1.1.2) can be established if $R_S / Z_0 = g_0 g_1 / \Delta$,

$R_L / Z_0 = g_N g_{N+1} / \Delta$, $M_{i,j} = \Delta / \sqrt{g_i g_j}$ for $i \neq j$, where Z_0 is the port impedance.

The values of g_n for $0 \leq n \leq N+1$ can be determined by the maximally-flat insertion

loss and return loss functions:

$$|S_{21}(\Omega)|^2 = \frac{1}{1+\Omega^{2N}} \tag{1.1.3a}$$

$$|S_{11}(\Omega)|^2 = \frac{\Omega^{2N}}{1+\Omega^{2N}} \tag{1.1.3b}$$

where N is the filter order. It can be seen that $|S_{21}|^2$ decreases monotonically with Ω

when $\Omega > 1$, and $|S_{11}|^2$ increases monotonically with Ω. A Chebyshev polynomial can

be used to specify the insertion loss and return loss of an N-order filter as

$$|S_{21}(\Omega)|^2 = \frac{1}{1+\varepsilon^2 C_N^2(\Omega)} \tag{1.1.4a}$$

$$|S_{11}(\Omega)|^2 = \frac{\varepsilon^2 C_N^2(\Omega)}{1+\varepsilon^2 C_N^2(\Omega)} \tag{1.1.4b}$$

where the ripple level of the in-band $|S_{21}|$ response is $10\log(1+\varepsilon^2)$ dB since the

Chebyshev polynomial $C_N(\Omega)$ oscillates when $-1 \leq \Omega \leq 1$. Design formulas for the

g_n in (1.1.2) based on (1.1.3) and (1.1.4) can be found in [1] and [12].

Fig. 1.2 shows the equivalent circuit incorporating multiple mutual inductive

coupling, and its impedance matrix can be expressed as [16]
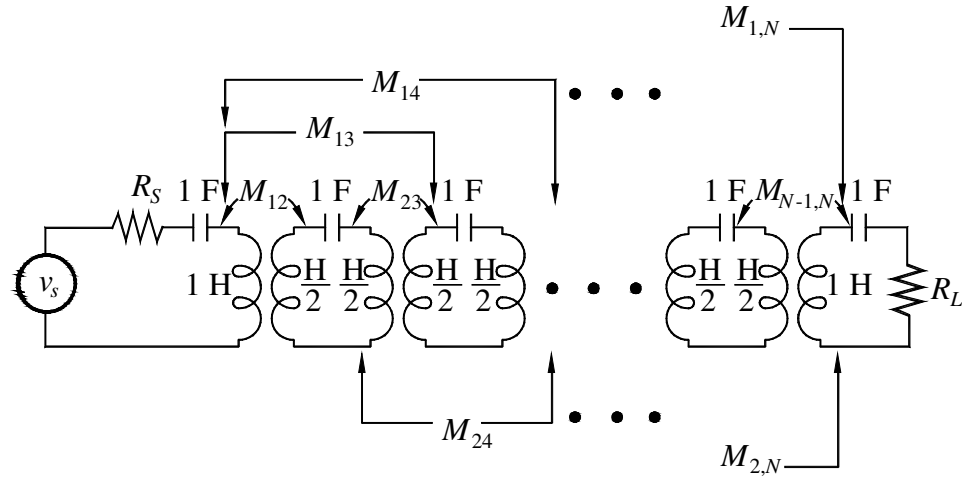
Fig. 1.2. The equivalent circuit of a direct-coupled waveguide filter incorporating multiple inductive coupling.

$$
\begin{bmatrix} v_s \\ 0 \\ 0 \\ \cdot \\ \cdot \\ 0 \\ 0 \end{bmatrix} = \begin{bmatrix} R_S + j\Omega & jM_{12} & jM_{13} & \cdot & \cdot & jM_{1,N-1} & jM_{1,N} \\ jM_{12} & j\Omega & jM_{23} & \cdot & \cdot & jM_{2,N-1} & jM_{2,N} \\ jM_{13} & jM_{23} & j\Omega & \cdot & \cdot & jM_{3,N-1} & jM_{3,N} \\ \cdot & \cdot & \cdot & \cdot & \cdot & \cdot & \cdot \\ \cdot & \cdot & \cdot & \cdot & \cdot & \cdot & \cdot \\ jM_{1,N-1} & jM_{2,N-1} & jM_{3,N-1} & \cdot & \cdot & j\Omega & jM_{N-1,N} \\ jM_{1,N} & jM_{2,N} & jM_{3,N} & \cdot & \cdot & jM_{N-1,N} & R_L + j\Omega \end{bmatrix} \begin{bmatrix} i_1 \\ i_2 \\ i_3 \\ \cdot \\ \cdot \\ i_{N-1} \\ i_N \end{bmatrix} \quad (1.1.5)
$$

Each resonator is not only coupled to the neighboring resonators in sequence, but also non-adjacent resonators by cross-coupling. The matrix in (1.1.5) can be written in a compact form:

$$
[Z] = [R] + j(\Omega[U] + [M]) \quad (1.1.6)
$$

where $[U]$ is an $N \times N$ identity matrix, $[R]$ has all zero entries except for (1, 1) and (N, N) elements. Matrix $[M]$ is called the coupling matrix and has elements of $M_{i,j}$ for $i \neq j$. This structure is particularly useful for the filters with pairs of transmission

zeros [14-19]. It is known that an impedance K-inverter, which can be equivalent to an inductive coupling element, is defined as [12]

$$\begin{bmatrix} v_1 \\ v_2 \end{bmatrix} = \begin{bmatrix} 0 & jK \\ jK & 0 \end{bmatrix} \begin{bmatrix} i_1 \\ i_2 \end{bmatrix} \tag{1.1.7}$$

By using the impedance K-inverter, the coupling between source/load and resonators can be taken into account by an extended $(N+2){\times}(N+2)$ matrix. In addition, it may be necessary to replace the frequency variable $j\Omega$ by $j(\Omega+X_i)$ for the (i, i) element in (1.1.5) if transmission zeros are not in pairs, i.e. the $|S_{21}|$ response is asymmetric with respect to the center frequency. Then, (1.1.5) is transformed to

$$\begin{bmatrix} v_s \\ 0 \\ 0 \\ . \\ . \\ 0 \\ 0 \end{bmatrix} = \begin{bmatrix} 1 & jK_{01} & jK_{02} & . & . & jK_{0,N} & jK_{0,N+1} \\ jK_{01} & j(\Omega+X_1) & jK_{12} & . & . & jK_{1,N} & jK_{1,N+1} \\ jK_{02} & jK_{12} & j(\Omega+X_2) & . & . & jK_{2,N} & jK_{2,N+1} \\ . & . & . & . & . & . & . \\ . & . & . & . & . & . & . \\ jK_{0,N} & jK_{1,N} & jK_{2,N} & . & . & j(\Omega+X_N) & jK_{N,N+1} \\ jK_{0,N+1} & jK_{1,N+1} & jK_{2,N+1} & . & . & jK_{N,N+1} & 1 \end{bmatrix} \begin{bmatrix} i_0 \\ i_1 \\ i_2 \\ . \\ . \\ i_N \\ i_{N+1} \end{bmatrix} \tag{1.1.8}$$

This matrix can be written in a compact form as

$$[Z] = [R] + j(\Omega[U] + [K]) \tag{1.1.9}$$

where $[R]$ has all zero elements except the $(1, 1)$ and $(N+2, N+2)$ elements, and
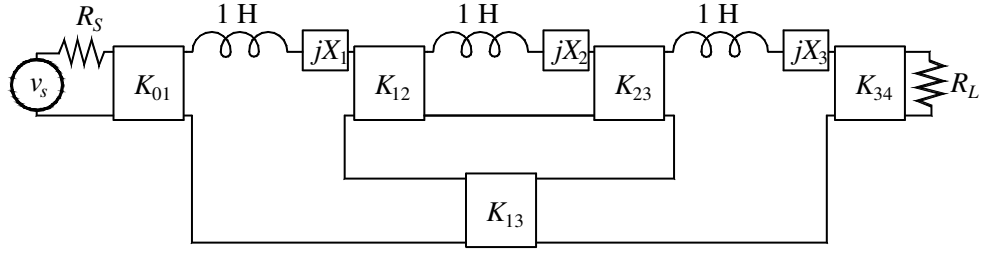
Fig. 1.3. The *K*-inverter equivalent circuit of a third-order filter.

$$[K] = \begin{bmatrix} 0 & K_{01} & K_{02} & . & . & K_{0,N} & K_{0,N+1} \\ K_{01} & X_1 & K_{12} & . & . & K_{1,N} & K_{1,N+1} \\ K_{02} & K_{12} & X_2 & . & . & K_{2,N} & K_{2,N+1} \\ . & . & . & . & . & . & . \\ . & . & . & . & . & . & . \\ K_{0,N} & K_{1,N} & K_{2,N} & . & . & X_N & K_{N,N+1} \\ K_{0,N+1} & K_{1,N+1} & K_{2,N+1} & . & . & K_{N,N+1} & 0 \end{bmatrix} \quad (1.1.10)$$

This matrix is frequently employed for synthesis of the waveguide filters since iris coupling between waveguide cavities can be properly modelled by the *K*-inverter. If the frequency variable Ω is viewed as a 1-H inductor, the lowpass prototype of a lossless filter can be obtained. For example, Fig. 1.3 shows the equivalent circuit of a lossless third-order filter with non-adjacent impedance inverter K_{13}.

For strip-transmission-line filters, however, the admittance matrix with *J*-inverters may be more suitable and can be expressed as [20]

$$\begin{bmatrix} v_s \\ 0 \\ 0 \\ . \\ . \\ 0 \\ 0 \end{bmatrix} = \begin{bmatrix} 1 & jJ_{01} & jJ_{02} & . & . & jJ_{0,N} & jJ_{0,N+1} \\ jJ_{01} & j(\Omega+B_1) & jJ_{12} & . & . & jJ_{1,N} & jJ_{1,N+1} \\ jJ_{02} & jJ_{12} & j(\Omega+B_2) & . & . & jJ_{2,N} & jJ_{2,N+1} \\ . & . & . & . & . & . & . \\ . & . & . & . & . & . & . \\ jJ_{0,N} & jJ_{1,N} & jJ_{2,N} & . & . & j(\Omega+B_N) & jJ_{N,N+1} \\ jJ_{0,N+1} & jJ_{1,N+1} & jJ_{2,N+1} & . & . & jJ_{N,N+1} & 1 \end{bmatrix} \begin{bmatrix} i_0 \\ i_1 \\ i_2 \\ . \\ . \\ i_N \\ i_{N+1} \end{bmatrix} \quad (1.1.11)$$

where the *J*-inverter is defined as [12]

$$\begin{bmatrix} i_1 \\ i_2 \end{bmatrix} = \begin{bmatrix} 0 & jJ \\ jJ & 0 \end{bmatrix} \begin{bmatrix} v_1 \\ v_2 \end{bmatrix}$$

(1.1.12)

The matrix in (1.1.11) can be expressed as

$$[Y] = [G] + j(\Omega[U] + [J])$$

(1.1.13)

where [*G*] has all zero elements except the (1, 1) and (*N*+2, *N*+2) elements, and

$$[J] = \begin{bmatrix} 0 & J_{01} & J_{02} & \cdot & \cdot & J_{0,N} & J_{0,N+1} \\ J_{01} & B_1 & J_{12} & \cdot & \cdot & J_{1,N} & J_{1,N+1} \\ J_{02} & J_{12} & B_2 & \cdot & \cdot & J_{2,N} & J_{2,N+1} \\ \cdot & \cdot & \cdot & \cdot & \cdot & \cdot & \cdot \\ \cdot & \cdot & \cdot & \cdot & \cdot & \cdot & \cdot \\ J_{0,N} & J_{1,N} & J_{2,N} & \cdot & \cdot & B_N & J_{N,N+1} \\ J_{0,N+1} & J_{1,N+1} & J_{2,N+1} & \cdot & \cdot & J_{N,N+1} & 0 \end{bmatrix}$$

(1.1.14)

If the frequency variable Ω is viewed as a 1-F capacitor, the lowpass prototype can be thus obtained. A third-order lowpass prototype is shown in Fig. 1.4, which is the dual of the circuit in Fig. 1.3.

The structures proposed to realize the filters with transmission zeros can be expressed by the coupling matrix [*M*] in (1.1.5), the *K*-inverter matrix [*K*] in (1.1.10), or the *J*-inverter matrix [*J*] in (1.1.14). Since the matrix [*J*] is particularly suitable for strip-transmission-line filters, and microstrip filters are used in the experiment in this study, the *J*-inverter equivalent circuit are adopted.
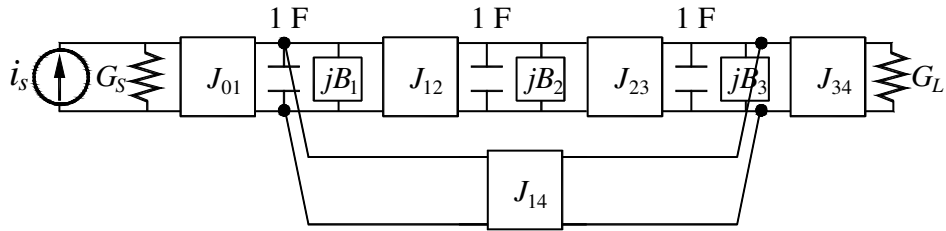
Fig. 1.4. The J-inverter equivalent circuit of a third-order filter.
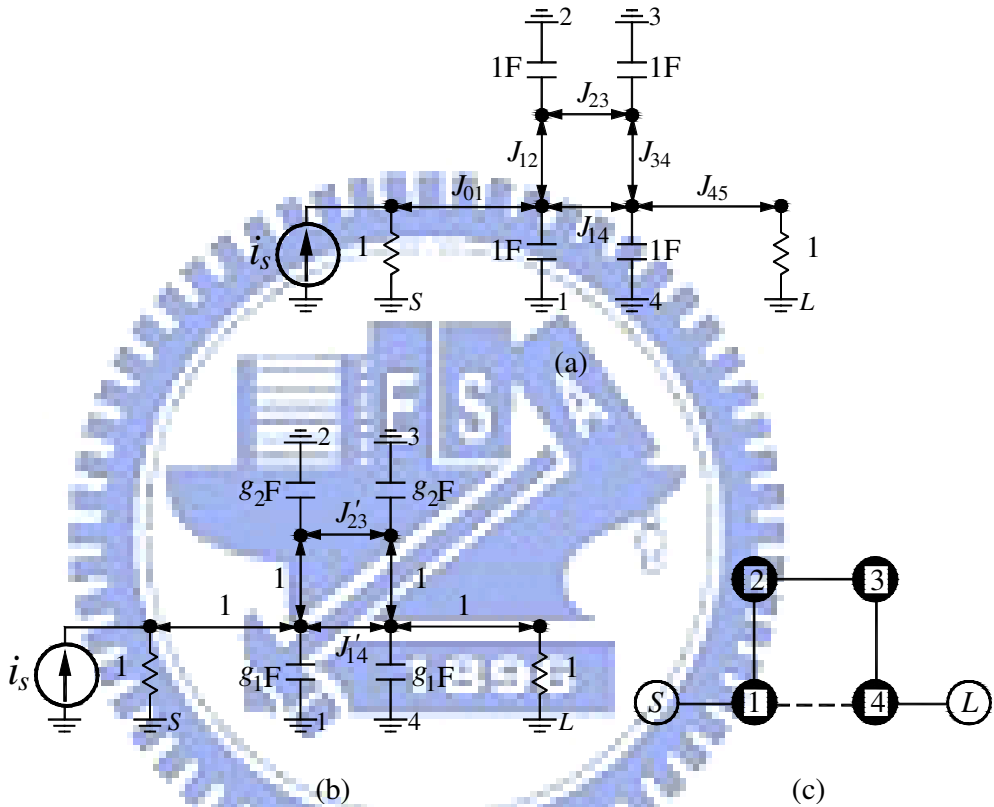
Fig. 1.5. The quadruplet filter. (a) The simplified form of the equivalent circuit. (b) The alternative equivalent circuit. (c) The coupling diagram.

For most of the practical microwave filters with transmission zeros, only a few non-adjacent coupling elements are required to establish. Take the quadruplet filter as an example [14, 15, 17-19, 21-23], Fig. 1.5(a) shows the simplified form of the equivalent circuit with six J-inverters: $J_{01}(J_{45}=J_{01})$, $J_{12}(J_{34}=J_{12})$, J_{14} and J_{23}. Note that

J_{13} and J_{24} inverters are not necessary in this network. Fig. 1.5(b) shows the alternative equivalent circuit, where the J_{01} and J_{12}-inverters are normalized to unity and the capacitances are changed accordingly. The equivalence between Fig. 1.5(a) and 1.5(b) can be established if $J_{01} = 1/\sqrt{g_1}$, $J_{12} = 1/\sqrt{g_1 g_2}$, $J_{23} = J'_{23}/g_2$, and $J_{14} = J'_{14}/g_1$. They can be obtained from the operations on the rows and columns of the following matrix.

$$[J] = \begin{bmatrix} 0 & J_{01} & 0 & 0 & 0 & 0 \\ J_{01} & 0 & J_{12} & 0 & J_{14} & 0 \\ 0 & J_{12} & 0 & J_{23} & 0 & 0 \\ 0 & 0 & J_{23} & 0 & J_{34} & 0 \\ 0 & J_{14} & 0 & J_{34} & 0 & J_{45} \\ 0 & 0 & 0 & 0 & J_{45} & 0 \end{bmatrix} \tag{1.1.15}$$

Fig. 1.5(c) plots the coupling diagram of the quadruplet, where the solid and the dashed lines represent mainline and cross coupling, respectively.

A number of coupling configurations based on the quadruplet (CQ) are devised for achieving a response with multiple pairs of transmission zeros [24-25]. The examples include the canonical form [24] and cascaded quadruplet (CQ) [25]. Fig. 1.6(a) and (b) plot the coupling diagrams, respectively. In these structures, multiple pairs of transmission zeros can be placed on the real axis or the imaginary axis. It is noted that no reactive element is added to the diagonal elements of the matrix [J], i.e. $B_i = 0$ for $1 \leq i \leq N$, since the distribution of transmission zeros are symmetric with respect to the real axis in the complex frequency plane.
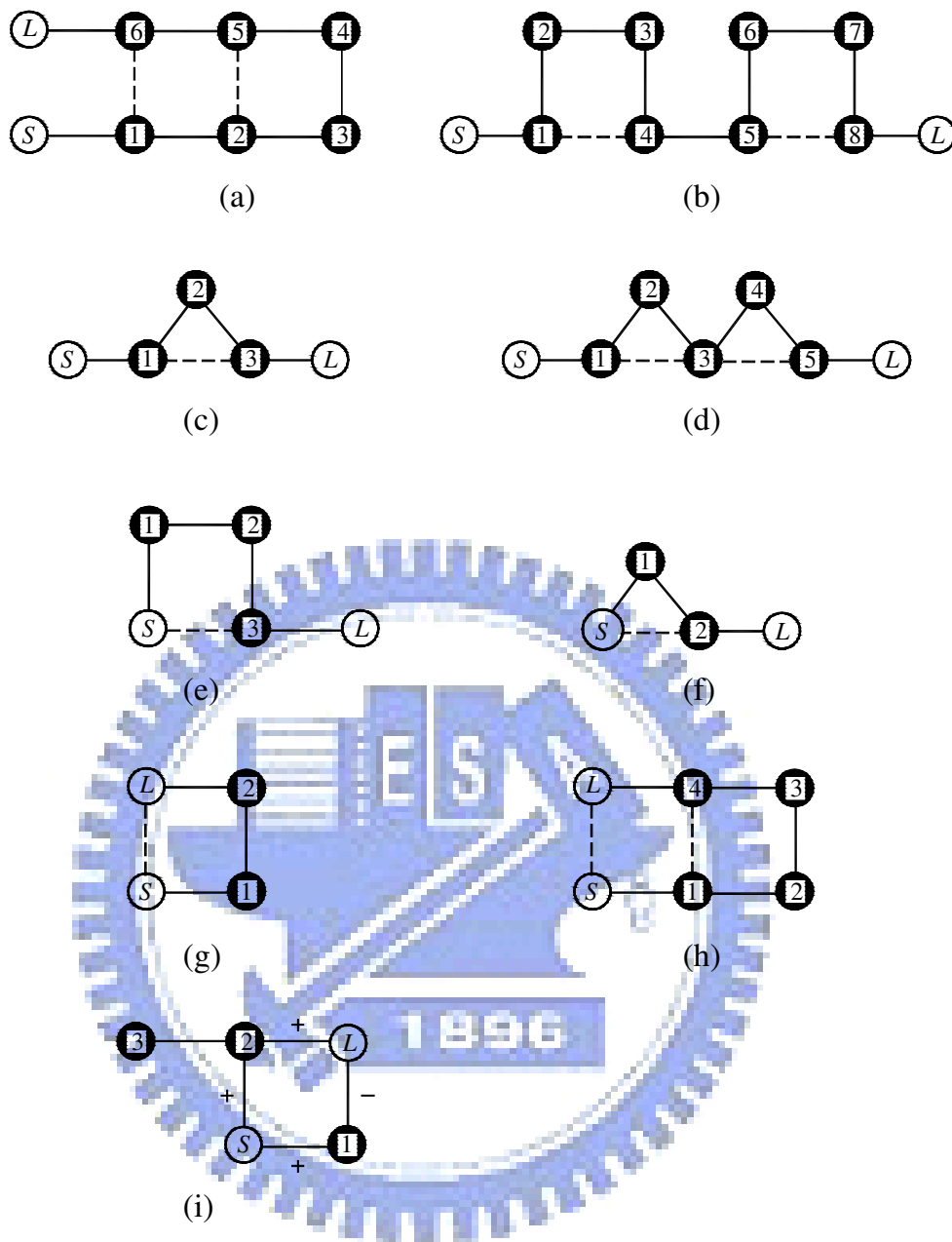
Fig. 1.6 Various coupling diagrams. (a) The canonical form of a sixth-order filter. (b) An eighth-order CQ filter. (c) The trisection filter. (d) A fifth-order CT filter. (e) A third-order filter with the source coupled to resonators 1 and 3. (f) A second-order filter with the he source coupled to resonators 1 and 2. (g) A second-order filter with source-load coupling. (h) The canonical form of a fourth-order filter with source-load coupling. (i) An extended doublet.

When the response is asymmetric with respect to the center frequency, the extracted-pole structure [26] and the trisection [27, 28] are proposed to realize a single transmission zero, respectively. The cascade trisection (CT) is useful for the higher order filters with an asymmetric response and multiple transmission zeros. Such filters can be applied to cellular base stations since the rejection on one side is more stringent than the other. Fig. 1.6(c) and (d) shows the coupling diagrams of the single trisection and a fifth-order CT filter, respectively.

In [29-31], the coupling from source/load to two resonators is proposed. For a third order network, a pair of transmission zeros can be generated if the source is simultaneously coupled to the first and the third resonators, as shown in Fig. 1.5(e) [29]. Compared with the quadruplet, the number of the resonators is reduced by one. For a second order network, a single transmission zero can be created if the source is coupled to two resonators, as shown in Fig. 1.5(f) [30]. Compared with a trisection, the number of resonators is reduced by one. An adaptive synthesis of coupled-resonator filters with source/load to multi-resonator coupling can be found in [31].

If direct coupling exists between source and load, it is shown that at most $N/2$ pairs of zeros can be generated for the canonical form with an N-even order [32-34]. Fig. 1.6(g) and (h) shows the coupling diagrams of the second-order and the fourth-order canonical form, respectively. The extended-doublet structure shown in Fig. 1.6(i) is a second realization of a third order filter with a pair of zeros [35, 36]. It consists of a main doublet attached by an additional resonator. The source and the load are coupled to two resonators in the main double. It is noted that the sign of one of the four coupling elements must be opposite to the others for generating a pair of

zeros. Waveguide cavities [35] and microstrip resonators [36] have been proposed to realize this structure.

1.2 Motivations

The motivation of this work roots in noting that many innovative coupled-resonator bandpass filters have been proposed to generate plural transmission zeros with fewer resonators [29-38]. Increasing number of transmission zeros around the passband can enhance the frequency selectivity so that the number of resonators can be reduced. This is accompanied with several advantages including lower insertion loss and a more compact circuit size. Many techniques have been proposed, which include source/load to multi-resonator coupling [29-31, 35, 36], source-load coupling [32-34], non-resonating nodes [35] and frequency-dependent coupling [37, 38].

In [29], a particular coupling scheme is arranged for source/load terminations and a triple-mode cavity to realize a third-order filter with a pair of zeros. In [30], the source and the load of a dual-mode resonator filter are designed to couple simultaneously to two resonators for creating two independently controllable zeros. In [34], fourth-order canonical microstrip filters with source-load coupling are developed to two pairs of zeros. In [35, 36], it is shown that an extended-doublet can generate a pair of zeros for a third-order filter. In [35], second and third-order coupled-cavity structures that can generate a pair of zeros can be cascaded by non-resonating nodes for higher-order waveguide filters with plural zeros. Note that all the structures involve source/load to multi-resonators coupling or source-load coupling. Theoretically, for a coupled-resonator filter of order N with

frequency-independent coupling, the maximum number of finite transmission zeros is at most N [32].

However, the number of transmission zeros can be increased by one if frequency-dependent coupling is used [37, 38]. In [37], a third-order waveguide filter is reported to have four zeros. The frequency-dependent coupling element consists of iris and waveguide stub element. Unfortunately, this structure can not be easily applied to transmission-line resonators. In [38], a second-order combline filter with a frequency-dependent dielectric capacitor between source and load is reported to have three zeros. It is noted that a general synthesis for the filters with frequency-dependent coupling has not been reported yet. This research aims at exploring frequency-dependent coupling structures capable of generating transmission zeros. In addition, filter synthesis with frequency-dependent coupling is developed.

From cost and circuit integration consideration, microstrip realization of bandpass filters has gained much attention [10]. The reduction of number of resonators is especially important to microstrip resonators since they have a relatively low quality (Q) factor. Many coupling diagrams have been applied to microstrip filters [22, 23, 28, 34, 36]. In [22, 23], a microstrip quadruplet is achieved by open-loop resonators. In [28], a fifth-order cascade trisection filter is realized by hairpin resonators. In [34], a short coupled-line is placed between input and output ports to introduce source-load coupling. In [36], a particular microstrip two-mode resonator accompanied by a hairpin resonator is proposed to realize a third-order filter with a pair of zeros.

In this work, microstrip frequency-dependent coupling structure is devised. Based on this structure, a microstrip trisection filter can have a pair of transmission zeros without using via-hole grounding, dual-mode resonating elements, and non-resonating nodes. Besides, source/load to multi-resonator coupling and source-load coupling are not required at all. Furthermore, the third-order filter can have two additional zeros created by tapped-line.

1.3 Contributions

A novel zero-generating structure with frequency-dependent coupling structure is developed. It has several attractive properties. First, the design is simple since the condition of zeros involves only two elements: a resonator and a frequency-dependent admittance inverter. Second, in the admittance matrix of the lowpass prototype, all diagonal elements are not required to add any reactive elements. Third, the trisection can be directly cascaded to other resonators by cross-coupling for higher order filters without using non-resonating nodes [35] or external components [38]. The formula of the lowpass prototypes with the proposed structure is developed. Microstrip filters of order $N = 3$ and 4 is designed to have at most four and five zeros, respectively.

It is found that this frequency-dependent coupling also exists among stepped-impedance resonators [39, 40] in a compact inline arrangement. All resonators form an in-line array so that the circuit occupies a compact area. When order is increased, the circuit size grows only in the direction of the width, which is usually much smaller than the length of the resonator. Furthermore, certain transmission zeros in the filter response can be generated by the nonadjacent

frequency-dependent coupling. Transmission zeros on both sides of the passband for fourth-, sixth-order filters are created by using proper non-adjacent coupling. Enhanced attenuation rate in transition bands is thus obtained.

Although the circuit layout looks quite similar to that of a combline structure, it needs neither lumped element nor grounding via, so that filter fabrication is easier and more reliable. The price paid for the full-length resonators is that circuit area is slightly larger than twice the size of a quarter-wave combline counterpart. The use of full-length resonators, however, brings one more degree of freedom to circuit designers in choosing symmetric or skew-symmetric feed [41]. It will be shown that existence and location of certain zeros are subject to the symmetry used in the tapped input/output arrangement. It is demonstrated for the particular in-line structure that the extra zero can be placed in lower and upper stopbands by symmetric and skew-symmetric feeds, respectively.

1.4 Organization of the Dissertation

Chapter 2 reviews the derivation of the general Chebyshev filtering function and the synthesis of several basic coupling schemes including quadruplet, trisection, and extended doublet. A novel zero-generating structure with frequency-dependent coupling is described in chapter 3. Three novel lowpass prototypes with a pair of transmission zeros are developed based on this structure. The design of the microstrip frequency-dependent J-inverter is given. The comparison of measured responses of experimental circuits with simulation data is also presented. In chapter 4, inline stepped-impedance resonator filters are explored. The existence of the zeros is studied in terms of Y-parameter matrix by taking the adjacent and nonadjacent

coupling into account. Creation of zeros by the tapped input/output structure is also investigated. Experiment is conducted to validate the theory. Finally, chapter 5 gives the conclusion.

18

This page is intentionally blank.
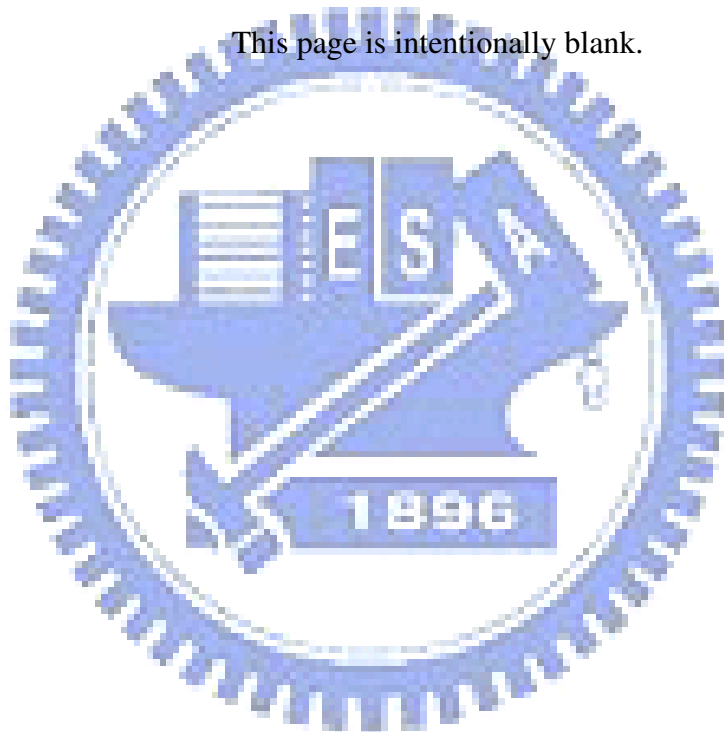
CHAPTER 2

Fundamental of Admittance Matrix Synthesis

In this chapter, synthesis of the admittance matrix for a filter with the general Chebyshev function is reviewed. Section 2.1 describes the technique for generating the Chebyshev polynomials with finite transmission zeros [11, 42]. Section 2.2 describes how to derive the *ABCD* matrix from the general Chebyshev filtering function. Finally, section 2.3 gives the synthesis of the admittance matrices for some basic coupling diagrams including quadruplet, trisection, and extended-doublet.

2.1 General Chebyshev Filtering Function

The general Chebyshev filtering function can be described by

$$C_N(\omega) = \cos\left[\sum_{n=1}^{N} \cos^{-1}(x_n(\omega))\right], |\omega| \le 1 \tag{2.1.1}$$

$$C_N(\omega) = \cosh\left[\sum_{n=1}^{N} \cosh^{-1}(x_n(\omega))\right], |\omega| \ge 1 \tag{2.1.2}$$

$$x_n(\omega) = \frac{\omega - 1/\omega_n}{1 - \omega/\omega_n} \tag{2.1.3}$$

where $j\omega_n = s_n$ is the location of the nth transmission zero in the complex plane. Since $x_n(1) = 1$ and $x_n(-1) = -1$, it is easily verified that $C_N(\omega)$ oscillates between -1 and 1. It is noted that $C_N(\omega)$ degenerates to the conventional Chebyshev function when all the transmission zeros are moved to the infinity. The number of finite

transmission zeros n_{fz} must be $\leq N$. The general Chebyshev function can be transformed to a polynomial by the operations as follows.

$$C_N(\omega) = \cosh\left[\sum_{n=1}^{N}\cosh^{-1}(x_n(\omega))\right] = \cosh\left[\sum_{n=1}^{N}\ln(a_n+b_n)\right] \tag{2.1.4}$$

$$a_n = x_n(\omega) = \frac{\omega - 1/\omega_n}{1-\omega/\omega_n} \quad\text{and}\quad b_n = \sqrt{x_n^2(\omega)-1} = \frac{\omega'\sqrt{1-\omega/\omega_n^2}}{1-\omega/\omega_n} \tag{2.1.5}$$

where $\omega' = \sqrt{\omega^2 - 1}$. Then (2.1.4) is transformed into

$$C_N(\omega) = \frac{1}{2}\left[e^{\sum_{n=1}^{N}\ln(a_n+b_n)} + e^{-\sum_{n=1}^{N}\ln(a_n+b_n)}\right] = \frac{1}{2}\left[\prod_{n=1}^{N}(a_n+b_n) + \frac{1}{\prod_{n=1}^{N}(a_n+b_n)}\right] \tag{2.1.6}$$

If the numerator and the denominator of the second term in (2.1.6) is multiplied by $\prod_{n=1}^{N}(a_n - b_n)$, we can obtain

$$C_N(\omega) = \frac{1}{2}\left[\prod_{n=1}^{N}(a_n+b_n) + \prod_{n=1}^{N}(a_n-b_n)\right] \tag{2.1.7}$$

Equation (2.1.7) can be further transformed into

$$C_N(\omega) = \frac{1}{2}\frac{\prod_{n=1}^{N}(c_n+d_n) + \prod_{n=1}^{N}(c_n-d_n)}{\prod_{n=1}^{n_{fz}}(1-\omega/\omega_n)} \tag{2.1.8}$$

$$c_n = \omega - \frac{1}{\omega_n} \quad\text{and}\quad d_n = \sqrt{\omega^2-1}\sqrt{1-1/\omega_n^2} \tag{2.1.9}$$

It can be seen that the roots the denominator of $C_N(\omega)$ are the transmission zeros. The numerator of $C_N(\omega)$ can be easily derived when $N \leq 4$. If $N = 3$, the numerator of $C_N(\omega)$ can be written as

$$\text{Num}[C_N(\omega)] = (c_1 c_2 + d_1 d_2)c_3 + (c_2 d_1 + c_1 d_2)d_3 \qquad (2.1.10)$$

If a transmission zero is placed at $s = j\omega_1$, it is obtained that $c_1 = c_2 = \omega$, $d_1 = d_2 = \omega'$,

$c_3 = \omega - \dfrac{1}{\omega_1}$, and $d_3 = \omega'\sqrt{1 - \dfrac{1}{\omega_1^2}}$. Then, (2.1.10) is derived as

$$\text{Num}[C_N(\omega)] = \omega^3\left(2 + 2\sqrt{1 - \frac{1}{\omega_1^2}}\right) + \omega^2\left(\frac{-2}{\omega_1}\right) + \omega\left(-1 - 2\sqrt{1 - \frac{1}{\omega_1^2}}\right) + \frac{1}{\omega_1} \quad (2.1.11)$$

Thus, the insertion loss function for a third-order filter with a transmission zero can be expressed as

$$|S_{21}|^2 = \frac{1}{1 + \varepsilon^2 C_3^2(\omega)} \qquad (2.1.12)$$

$$C_3(\omega) = \frac{b_3\omega^3 + b_2\omega^2 + b_1\omega + b_0}{a_1\omega + a_0} \qquad (2.1.13)$$

where the coefficients are $a_0 = 1$, $a_1 = -1/\omega_1$, $b_0 = 1/\omega_1$, $b_1 = -1 - 2\sqrt{1 - 1/\omega_1^2}$,

$b_2 = -2/\omega_1$, and $b_3 = 2 + 2\sqrt{1 - 1/\omega_1^2}$.

If a pair transmission zeros are symmetrically placed at $s = \pm j\omega_1$ on the imaginary axis in the complex plane, then $c_1 = \omega + \dfrac{1}{\omega_1}$, $d_1 = \omega'\sqrt{1 - \dfrac{1}{\omega_1^2}}$, $c_2 = \omega - \dfrac{1}{\omega_1}$, $d_2 = \omega'\sqrt{1 - \dfrac{1}{\omega_1^2}}$, $c_3 = \omega$, and $d_3 = \omega'$. Then,

$$\mathrm{Num}[C_N(\omega)] = \omega^3 \left(2 - \frac{1}{\omega_1^2} + 2\sqrt{1 - \frac{1}{\omega_1^2}} \right) - \omega \left(1 + 2\sqrt{1 - \frac{1}{\omega_1^2}} \right) \qquad (2.1.14)$$

The general Chebyshev function for a third-order filter with a pair of zeros at $s = \pm j\omega_1$ can be thus expressed as

$$C_3(\omega) = \frac{b_3\omega^3 + b_1\omega}{a_2\omega^2 + a_0} \qquad (2.1.15)$$

where the coefficients are $a_0 = 1$, $a_2 = -1/\omega_1^2$, $b_1 = -1 - 2\sqrt{1 - 1/\omega_1^2}$, and $b_3 = 2 - 1/\omega_1^2 + 2\sqrt{1 - 1/\omega_1^2}$.

If the pair of zeros is placed on the real axis at $s = \pm\omega_1$, it is easy to obtain the coefficient: $a_0 = 1$, $a_2 = 1/\omega_1^2$, $b_1 = -1 - 2\sqrt{1 + 1/\omega_1^2}$, and $b_3 = 2 + 1/\omega_1^2 + 2\sqrt{1 + 1/\omega_1^2}$.

The general Chebyshev function for a fourth-order filter with a pair of zeros at $s = \pm j\omega_1$ can be derived in a similar manner and be expressed as

$$C_4(\omega) = \frac{b_4\omega^4 + b_2\omega^2 + b_0}{a_2\omega^2 + a_0} \qquad (2.1.16)$$

where $a_0 = 1$, $a_2 = -1/\omega_1^2$, $b_0 = 1$, $b_2 = -4 + 1/\omega_1^2 - 4\sqrt{1 - 1/\omega_1^2}$, and

$b_4 = 2 + 2(1 - 1/\omega_1^2) + 4\sqrt{1 - 1/\omega_1^2}$.

In fact, the higher order Chebyshev polynomials with plural transmission zeros can be obtained by a recursive procedure [42]. The algorithm starts with

$$U_1(\omega) = \omega - \frac{1}{\omega_1} \quad \text{and} \quad V_1(\omega) = \sqrt{1 - \frac{1}{\omega_1^2}} \tag{2.1.17}$$

where the $s = j\omega_1$ is the location of the first zero. Then, the process continues with the following equations until all the zeros are used.

$$U_n(\omega) = \left(\omega - \frac{1}{\omega_n}\right) U_{n-1}(\omega) + (\omega^2 - 1)\sqrt{1 - \frac{1}{\omega_n^2}} V_{n-1}(\omega) \tag{2.1.18}$$

$$V_n(\omega) = \left(\omega - \frac{1}{\omega_n}\right) V_{n-1}(\omega) + \sqrt{1 - \frac{1}{\omega_n^2}} U_{n-1}(\omega) \tag{2.1.19}$$

If the order of the general Chebyshev function is N, the numerator can be expressed as

$$\text{Num}[C_N(\omega)] = U_N(\omega) \tag{2.1.20}$$

This algorithm can be programmed for computers without difficulties. In summary, the general Chebyshev filtering function with a total of n_{fz} zeros can be expressed by a rational form with denominator and numerator polynomials.

2.2 Synthesis of the *ABCD* Matrix

The next step to synthesize the admittance matrix of a filter is to obtain the *ABCD* parameters, which are assumed functions of complex frequency variable *s*. The derivation starts from obtaining the $S_{21}(s)$ from the insertion loss function by substituting $(-js)$ for ω

$$|S_{21}(s)|^2 = \frac{1}{1+\varepsilon^2 C_N^2(\omega)}\bigg|\omega = -js \qquad (2.2.1)$$

To form the function $S_{21}(s)$ from the given $|S_{21}(s)|^2$, the right half-plane poles are rejected, and the left-plane poles are used to derive

$$S_{21}(s) = \frac{P(s)}{\varepsilon_I F(s)} \qquad (2.2.2)$$

where polynomial $P(s)$ and $F(s)$ are normalized so that their highest coefficients are unity, and ε_I can be derived by

$$\varepsilon_I = \varepsilon \frac{P(s)}{F(s)}\bigg|s = j \qquad (2.2.3)$$

In a similar manner, the function $S_{11}(s)$ can be obtained from

$$|S_{11}(s)|^2 = \frac{\varepsilon^2 C_N^2(\omega)}{1+\varepsilon^2 C_N^2(\omega)}\bigg|\omega = -js \qquad (2.2.4)$$

Noting that $S_{21}(s)$ and $S_{11}(s)$ must have the same denominator, $S_{11}(s)$ can be expressed as

$$S_{11}(s) = \frac{E(s)}{\varepsilon_R F(s)} \qquad (2.2.5)$$

where the polynomial $E(s)$ is also normalized so that the highest coefficients are unity. If there are zeros at infinity, i.e. $n_{fz} < N$, it can be seen that $S_{11}(s) = \pm 1$ when s approaches infinity. Thus, we have $\varepsilon_R = \pm 1$ since the highest coefficients of $E(s)$ and $F(s)$ are unity. This condition holds for most cases studied in this research.

Based on the conversion from S-parameters to *ABCD* parameters, the *ABCD* matrix for a filter with the general Chebyshev response can be expressed as

$$[ABCD] = \frac{1}{P(s)/\varepsilon_I} \begin{bmatrix} A(s) & B(s) \\ C(s) & D(s) \end{bmatrix} \qquad (2.2.6)$$

The polynomials $A(s)$, $B(s)$, $C(s)$, and $D(s)$ can be generally expressed as

$$A(s) = j\,\mathrm{Im}(e_N + f_N)s^N + \mathrm{Re}(e_{N-1} + f_{N-1})s^{N-1} + j\,\mathrm{Im}(e_{N-2} + f_{N-2})s^{N-2} + \dots \qquad (2.2.7)$$

$$B(s) = \mathrm{Re}(e_N + f_N)s^N + j\,\mathrm{Im}(e_{N-1} + f_{N-1})s^{N-1} + \mathrm{Re}(e_{N-2} + f_{N-2})s^{N-2} + \dots \qquad (2.2.8)$$

$$C(s) = \mathrm{Re}(e_N - f_N)s^N + j\,\mathrm{Im}(e_{N-1} - f_{N-1})s^{N-1} + \mathrm{Re}(e_{N-2} - f_{N-2})s^{N-2} + \dots \qquad (2.2.9)$$

$$D(s) = j\,\mathrm{Im}(e_N - f_N)s^N + \mathrm{Re}(e_{N-1} - f_{N-1})s^{N-1} + j\,\mathrm{Im}(e_{N-2} - f_{N-2})s^{N-2} + \dots \qquad (2.2.10)$$

where e_i an f_i, $i = 0, 1, 2, \dots, N\text{-}1$ are the coefficients of $E(s)$ and $F(s)$, respectively.

$$E(s) = s^N + e_{N-1}s^{N-1} + \ldots + e_2s^2 + e_1s + e_0 \tag{2.2.11}$$

$$F(s) = s^N + f_{N-1}s^{N-1} + \ldots + f_2s^2 + f_1s + f_0 \tag{2.2.12}$$

Noting that $\varepsilon_R = 1$ in (2.2.5), it can be observed that $B(s)$ is of degree N, $A(s)$ and $D(s)$ are of degree N-1. Since the network is reciprocal, the degree of $C(s)$ must be N–2. This matrix is suitable for a network of even-N degree. If the coefficient $\varepsilon_R = -1$, $A(s)$ and $D(s)$ are still of degree N–1. However, $C(s)$ and $B(s)$ become the polynomials of degree N and N–2, respectively. This matrix is used for a network of odd-N degree.

If a pair of transmission zeros is specified at $s = \pm j3$ and in-band ripple is 0.1dB for a filter of $N = 3$, the polynomials can be derived as $A(s) = D(s) = 1.9007s^2 + 1.73596$, $B(s) = 1.7877s$, and $C(s) = 2s^3 + 3.3167s$. For the purpose of network synthesis, the product of the constant terms in $A(s)$ and $D(s)$ is intentionally normalized to unity. This normalization leads to
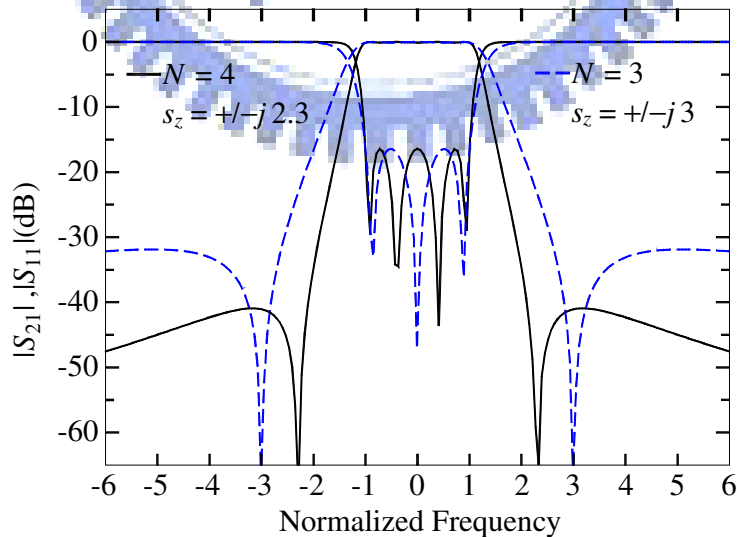
Fig. 2.1. The responses of lowpass prototype networks.

$$A(s) = D(s) = 1.0949s^2 + 1 \qquad (2.2.13)$$

$$B(s) = 1.0298s \qquad (2.2.14)$$

$$C(s) = 1.1521s^3 + 1.9106s. \qquad (2.2.15)$$

Fig. 2.1 plots the $|S_{21}|$ and $|S_{11}|$ responses of this filter. Also shown in Fig. 2.1 is the responses for a filter of $N = 4$ with a pair of transmission zeros at $s = \pm j2.3$ and in-band ripple is 0.1dB, the polynomials are as follows: $A(s) = D(s) = 1.7807s^3 + 2.0487s$, $B(s) = 2s^4 + 3.6378s^2 + 1.0559$, $C(s) = 1.5854s^2 + 0.7791$. For enforcing the product of the constant terms in $B(s)$ and $C(s)$ to unity, all the polynomials are multiplied by a constant 1.1025. Then, we obtain

$$A(s) = D(s) = 1.9633s^3 + 2.2588s \qquad (2.2.16)$$

$$B(s) = 2.2051s^4 + 4.0108s^2 + 1.1642 \qquad (2.2.17)$$

$$C(s) = 1.7482s^2 + 0.85896 \qquad (2.2.18)$$

It is noted that all the coefficients are real since the distribution of the roots of $E(s)$ and $F(s)$ is symmetric with respect to the real axis of the complex plane.

2.3 Synthesis of the Admittance Matrix

2.3.1 Quadruplet and Its Variants

Fig. 2.2 shows the generic block which is the basic structure for a quadruple to generate a pair of transmission zeros. The creation of transmission zeros is explained as follows. The circuit in Fig. 2.2 has two signal paths between input and output ports. One is by the J_x-inverter, which is realized by cross-coupling, and its Y-parameter matrix can be expressed as

(a)   (b)
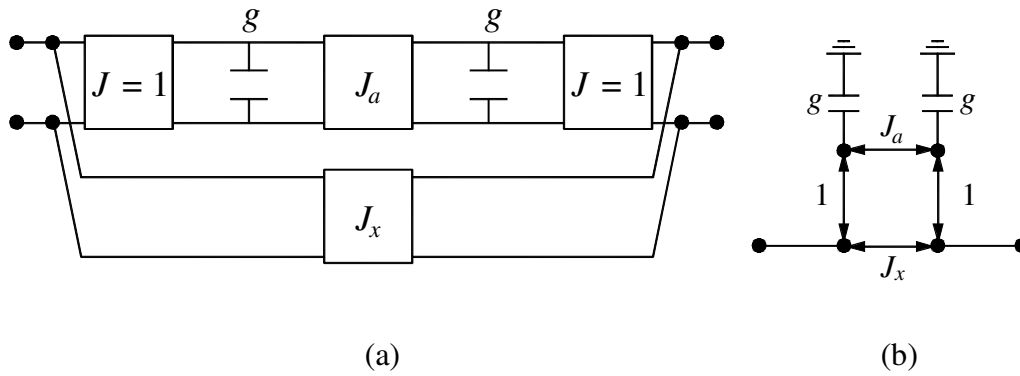
Fig. 2.2. The basic structure of a quadruplet. (a) The *J*-inverter circuit. (b) The simplified schematic.

$$[Y] = jJ_x \begin{bmatrix} 0 & 1 \\ 1 & 0 \end{bmatrix}$$

(2.3.1)

The other path is a cascade of two unitary *J*-inverters, two shunt capacitors *g* with an in-between J_a-inverter. *Y*-parameter matrix of this path from the input to the output can be expressed as

$$[Y] = \frac{1}{J_a + g^2 s^2 / J_a} \begin{bmatrix} gs/J_a & -j \\ -j & gs/J_a \end{bmatrix}$$

(2.3.2)

The transmission zeros can be obtained by enforcing $Y_{21} = Y_{12}$ of the entire network to zero. The condition can be explicitly expressed as [21-23]

$$s^2 = \frac{J_a(1 - J_x J_a)}{J_x g^2}$$

(2.3.3)

It is evident that a pair of zeros can be symmetrically generated on the imaginary

axis in the complex frequency plane at $s = \pm j\Omega_z$ if the relation $J_a/J_x < 0$ holds since $1 - J_x J_a > 0$. On the other hand, the zeros can be shifted to $s = \pm \Omega_z$ by simply reversing the sign of J_a/J_x. The *ABCD* matrix of the whole circuit can be expressed as

$$
\begin{bmatrix} A & B \\ C & D \end{bmatrix} = \frac{j}{\dfrac{J_x g^2}{J_a K} s^2 + 1} \begin{bmatrix} \dfrac{g}{J_a K} s & \dfrac{g^2}{J_a K} s^2 + \dfrac{J_a}{K} \\ \dfrac{J_x^2 g^2}{J_a K} s^2 + \dfrac{K}{J_a} & \dfrac{g}{J_a K} s \end{bmatrix}
\tag{2.3.4}
$$

where $K = J_x J_a - 1$. The *ABCD* matrix can be used in the synthesis of a filter based on this block.

Fig. 2.3 plots three possible schematics based on the zero-generating block described by (2.3.4). The circuit in Fig. 2.3(a) is the conventional quadruplet, the *ABCD* matrix of which can be expressed as

(a) (b) (c)
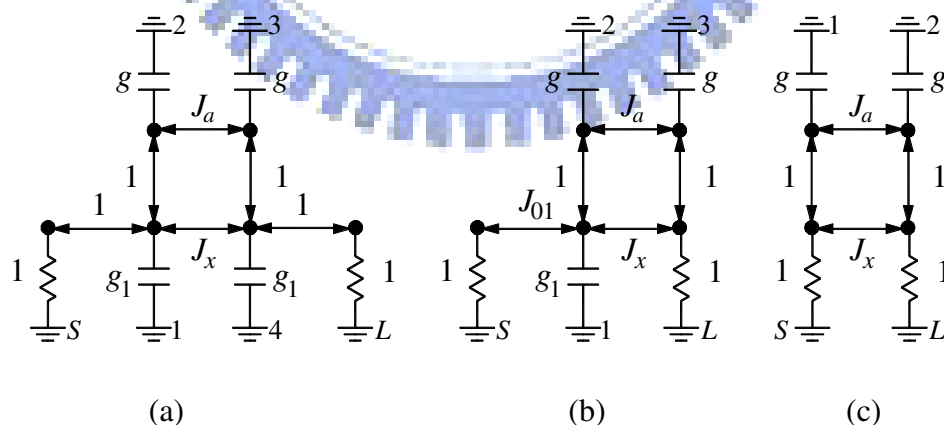
Fig. 2.3. The quadruplet and its variants. (a) The conventional quadruplet. (b) The circuit in which the load is simultaneously coupled to two resonators. (c) The circuit including the source-load coupling.

$$A(s) = D(s) = \frac{g_1 g^2}{J_a K} s^3 + \left(\frac{g}{J_a K} + \frac{J_a}{K} g_1 \right) s \tag{2.3.5}$$

$$B(s) = \frac{g_1^2 g^2}{J_a K} s^4 + \frac{1}{J_a K} \left(g_1 g + \left(1 + J_x^2 \right) g^2 + g_1^2 J_a^2 \right) s^2 + \frac{K}{J_a} \tag{2.3.6}$$

$$C(s) = \frac{g^2}{J_a K} s^2 + \frac{J_a}{K} \tag{2.3.7}$$

Comparing the coefficients in (2.3.5-7) with those in (2.2.16-18), one can obtain the element values.

The circuit in Fig. 3(b) is a third-order filter with a pair of transmission zeros. Although the load is requited to simultaneously couple to the first and the third resonators, the number of the resonators is reduced by one. The *ABCD* matrix can be expressed as

$$A(s) = \frac{1}{J_{01}} \left(\frac{g_1 g + J_x^2 g^2}{J_a K} s^2 + \frac{K}{J_a} \right) \tag{2.3.8}$$

$$B(s) = \frac{1}{J_{01}} \left(\frac{g_1 g^2}{J_a K} s^3 + \left(\frac{J_a g_1}{K} + \frac{g}{J_a K} \right) s \right) \tag{2.3.9}$$

$$C(s) = J_{01} \frac{g}{J_a K} s \tag{2.3.10}$$

$$D(s) = J_{01} \left(\frac{g^2}{J_a K} s^2 + \frac{J_a}{K} \right) \tag{2.3.11}$$

By comparing (2.3.8-11) and (2.2.13-15), the element values can be determined. The circuit in Fig. 3(c) uses only two resonators to achieve a pair of transmission zeros. However, this structure can not be directly cascaded with other resonators. In addition, the design of source-load coupling may not be as well-known as that of the

inter-resonator coupling. It is noted that ε_R is no longer unity, which will be determined by the $|S_{21}|$ level at infinity.

2.3.2 Extended-Doublet

Another three-resonator structure to produce a pair of zeros is the extended-doublet, as shown in Fig. 2.4(a). The generic block to produce a pair of zeros is shown in Fig. 2.4(b). It is noted that the generic block of the extended doublet requires three resonators. In fact, the resonator number compared with that of a quadruplet is increased by one. The generic structure can be analyzed as follows. The Y-parameter matrix of the route through resonator 1 can be expressed as

$$[Y] = \frac{J_{01}^2}{s}\begin{bmatrix} 1 & -1 \\ -1 & 1 \end{bmatrix} \qquad (2.3.12)$$

The other route with two resonators can be expressed as

$$[Y] = \frac{J_{02}^2}{s + J_{23}^2/s}\begin{bmatrix} 1 & 1 \\ 1 & 1 \end{bmatrix} \qquad (2.3.13)$$

The transmission zeros can be obtained by enforcing $Y_{21} = Y_{12}$ of the entire network to zero. The condition can be explicitly expressed as

$$s^2 = \frac{J_{01}^2 J_{23}^2}{J_{02}^2 - J_{01}^2} \qquad (2.3.14)$$

(a)   (b)
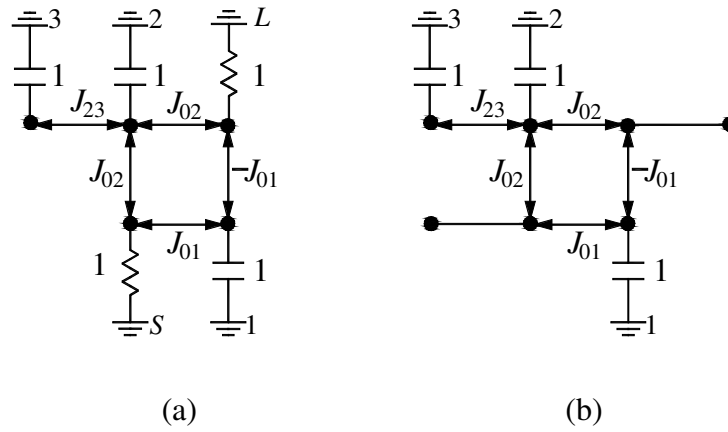
Fig. 2.4. The extended-double. (a) The schematic. (b) The generic block to produce a pair of zeros.

It can be seen that the location of zeros is controlled by the sign of $J_{02}^2 - J_{01}^2$. The *ABCD* matrix of the whole circuit can be expressed as

$$\begin{bmatrix} A & B \\ C & D \end{bmatrix} = \frac{1}{\dfrac{J_{01}^2 - J_{02}^2}{J_{01}^2 J_{23}^2} s^2 + 1} \begin{bmatrix} \dfrac{J_{01}^2 + J_{02}^2}{J_{01}^2 J_{23}^2} s^2 + 1 & \dfrac{1}{J_{01}^2 J_{23}^2} s^3 + \dfrac{1}{J_{01}^2} s \\ 4\dfrac{J_{02}^2}{J_{23}^2} & \dfrac{J_{01}^2 + J_{02}^2}{J_{01}^2 J_{23}^2} s^2 + 1 \end{bmatrix} \tag{2.3.15}$$

The structures in Fig. 2.3(b) and Fig. 2.4(a) can be used to generate a pair of zeros for a third-order filter. However, both schematics involve source/load to multi-resonator coupling. One may wonder whether it is possible to devise a third-order filter with only inter-resonator coupling to produce a pair of zeros.

2.3.3 Trisection

For completeness of this chapter, the analysis of the trisection is also presented. Fig. 2.5(a) shows that a shunt-connected pair $sg+jB$ is placed between any two *J*-inverters. The generic structure for generating the single transmission zero is

plotted in Fig. 2.5(b). The *Y*-parameter of the cross-coupling path can be expressed as

$$[Y] = jJ_x \begin{bmatrix} 0 & 1 \\ 1 & 0 \end{bmatrix} \tag{2.3.16}$$

The *Y*-parameter matrix of the other path is

$$[Y] = \frac{1}{sg + jB} \begin{bmatrix} 1 & 1 \\ 1 & 1 \end{bmatrix} \tag{2.3.17}$$

The transmission zeros can be easily derived by enforcing $Y_{21} = Y_{12}$ of the entire network to zero. The condition is

$$s = j\frac{1 - J_x B}{gJ_x} \tag{2.3.18}$$
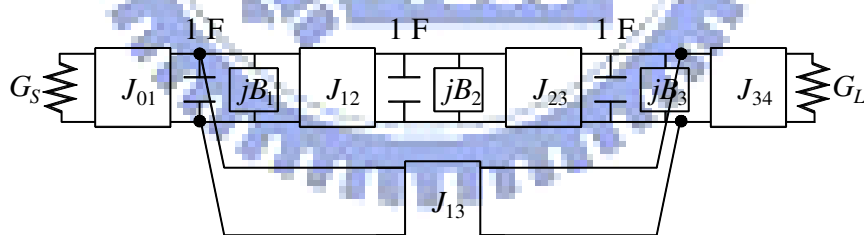
(a)
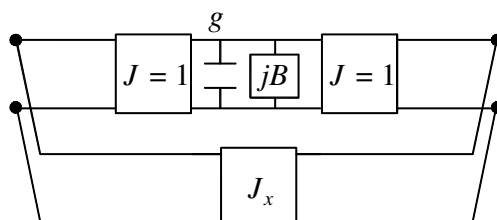
(b)

Fig. 2.5. The conventional trisection. (a) The *J*-inverter circuit. (b) The generic structure to produce a single transmission zero.

Since $g > 0$ and $1-J_xB > 0$, the single zero can be placed in the upper rejection band

if $J_x > 0$. On the contrary, the single zero can be placed in the lower rejection band

when $J_x < 0$. The *ABCD* matrix of the structure in Fig. 2.5(b) can be expressed as

$$\begin{bmatrix} A & B \\ C & D \end{bmatrix} = \frac{-1}{jgJ_xs+(1-J_xB)} \begin{bmatrix} 1 & sg+jB \\ gJ_x^2s - jJ_x(2-JB) & 1 \end{bmatrix} \qquad (2.3.19)$$

From (2.1.13), one can derive the *ABCD* matrix for a third-order filter with 0.1-dB

in-band ripple and a single transmission zero at $s = j3$.

$$\begin{bmatrix} A & B \\ C & D \end{bmatrix} = \begin{bmatrix} 1.2476s^2 - j0.2974s + 1 & 1.2095s - j0.3692 \\ 1.2868s^3 - j0.2207s^2 + 2.1652s - j0.4796 & 1.2476s^2 - j0.2974s + 1 \end{bmatrix}$$

$$(2.3.20)$$

Based on (2.3.19), the admittance matrix can be directly obtained as

$$[Y] = \begin{bmatrix} 1 & j0.9847 & 0 & 0 & 0 \\ j0.9847 & s+j0.0668 & j0.8838 & j0.2899 & 0 \\ 0 & j0.8838 & s-j0.3053 & j0.8838 & 0 \\ 0 & j0.2899 & j0.8838 & s+j0.0668 & j0.9847 \\ 0 & 0 & 0 & j0.9847 & 1 \end{bmatrix} \qquad (2.3.21)$$

Then, the coupling coefficients and loaded Q factors for the coupled-resonator filter

can be immediately obtained from (2.3.21).

CHAPTER 3

Synthesis and Microstrip Realization of Filters with Frequency-Dependent Admittance Inverters

In this chapter, we explore a novel structure with frequency-dependent admittance J-inverter to generate a pair of transmission zeros. This configuration involves only two elements: a resonator and a frequency-dependent admittance inverter. In the admittance matrix of the lowpass prototype, all diagonal elements are not required to add any reactive elements. This property is different from that of a conventional trisection. Furthermore, the trisection can be directly cascaded to other resonators by cross-coupling. Section 3.1 explains the generation of a pair of zeros. Section 3.2 describes the synthesis of lowpass prototypes based on the proposed trisection. The element values are derived by comparing the coefficients of the polynomials in the two-port $ABCD$ matrix with those derived from the general Chebyshev filtering function. Section 3.3 addresses the microstrip design of the J-inverters. Section 3.4 compares measured responses of experimental circuits with simulation data.

3.1 Frequency-Dependent J-Inverter for Generating a Pair of Zeros

Fig. 3.1 shows two possible blocks which can generate a pair of transmission zeros using frequency-dependent J-inverters. The frequency dependence is represented by a complex frequency variable s. The generation of transmission zeros is explained as follows. The circuit in Fig. 3.1(a) has two signal paths between input and output ports. One is the frequency-dependent J-inverter and the other is a cascade of two unitary J-inverters with a shunt capacitor $C = sg$ in between. The

Y-matrix of the upper path is

$$[Y] = sJ \begin{bmatrix} 0 & 1 \\ 1 & 0 \end{bmatrix} \tag{3.1.1}$$

The lower path can be expressed as

$$[Y] = \frac{1}{sg} \begin{bmatrix} 1 & 1 \\ 1 & 1 \end{bmatrix} \tag{3.1.2}$$

The condition of transmission zeros can be obtained by enforcing $Y_{21} = Y_{12}$ of the entire network to zero and can be explicitly expressed as

$$s^2 = -\frac{1}{Jg} \tag{3.1.3}$$

It is evident that a pair of zeros can be symmetrically generated on the imaginary axis in the complex frequency plane at $s = \pm j\Omega_z$ if the relation $Jg > 0$ holds and $\Omega_z = 1/\sqrt{Jg}$. On the other hand, the zeros can be shifted to $s = \pm\Omega_z$ by simply inverting the sign of *Jg*. The *ABCD* matrix of the whole circuit can be expressed as

(a)　　　　　　　　　　　　(b)
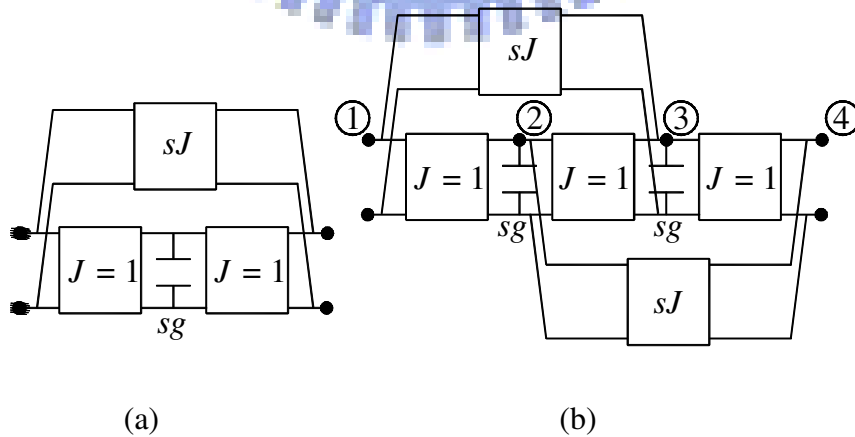
Fig. 3.1. Two circuits with frequency-dependent *J*-inverter for generating a pair of zeros. (a) Single trisection. (b) Two trisections.

$$\begin{bmatrix} A & B \\ C & D \end{bmatrix} = \frac{1}{1+s^2 Jg} \begin{bmatrix} -1 & -sg \\ sJ(2+s^2 Jg) & -1 \end{bmatrix} \qquad (3.1.4)$$

Fig. 3.1(b) shows an alternative structure for creating a pair of zeros on both sides of the passband. The zero condition can be derived as follows. As shown in Fig. 3.1(b), the circuit can be viewed as a four-port. Its Y-matrix can be expressed as

$$\begin{bmatrix} 0 & j & sJ & 0 \\ j & sg & j & sJ \\ sJ & j & sg & j \\ 0 & sJ & j & 0 \end{bmatrix} \begin{bmatrix} v_1 \\ v_2 \\ v_3 \\ v_4 \end{bmatrix} = \begin{bmatrix} i_1 \\ i_2 \\ i_3 \\ i_4 \end{bmatrix} \qquad (3.1.5)$$

where i_j represents the current flowing into nodes j and v_j represents the voltage at nodes j. Then, Reducing the four-pot to a two-port can be achieved by setting ports 2 and 3 open circuit by letting $i_2 = i_3 = 0$. By enforcing $Y_{21} = 0$ of the two-port circuit, the condition of the transmission zeros can be obtained as

$$s^2 = -\frac{1}{2gJ - J^2} \qquad (3.1.6)$$

This structure is advantageous for even-order filters since the circuit is symmetric. Besides, it can be seen from (3.1.6) that the value of the J-inverter is approximately a half of that in (3.1.3) for a prescribed Ω_z. The polynomials in the $ABCD$ matrix of the circuit in Fig. 3.1(b) involve terms of degree $n > 2$. However, the polynomials can be simplified when $J \ll g$. This approximation leads to the expression as

$$\begin{bmatrix} A & B \\ C & D \end{bmatrix} = \frac{j}{1 + s^2\left(2Jg - J^2\right)} \begin{bmatrix} s(g - 2J) & 1 \\ s^2 g^2 + 1 & s(g - 2J) \end{bmatrix} \qquad (3.1.7)$$

This matrix is not strictly reciprocal since $AD - BC \neq 1$. However, the deviation is small and the approximation is accurate enough for filter synthesis.

3.2 Synthesis of Lowpass Prototypes

Fig. 3.2 plots three possible lowpass prototypes based on the proposed zero-generating blocks. For the third-order network in Fig. 2(a), the *ABCD* matrix can be expressed as

$$A(s) = D(s) = g_2 g_3 s^2 + 1 \qquad (3.2.1)$$

$$B(s) = g_2 s \qquad (3.2.2)$$

$$C(s) = \left(g_1 g_2 g_3 - \frac{J_{13}^2}{g_2} \right) s^3 + \left(g_1 + g_3 - 2J_{13} \right) s \qquad (3.2.3)$$

If Ω_z is specified at $s = \pm j3$ and in-band ripple is 0.1dB, it has been shown in (2.2.13-15) that the polynomials are $A(s) = D(s) = 1.0949s^2 + 1$, $B(s) = 1.0298s$, and $C(s) = 1.1521s^3 + 1.9106s$. Thus, provided $g_1 = g_3$, the element values g_1, g_2 and J_{13} can be analytically derived and the admittance matrix of the network in Fig. 3.2(a) can be expressed as
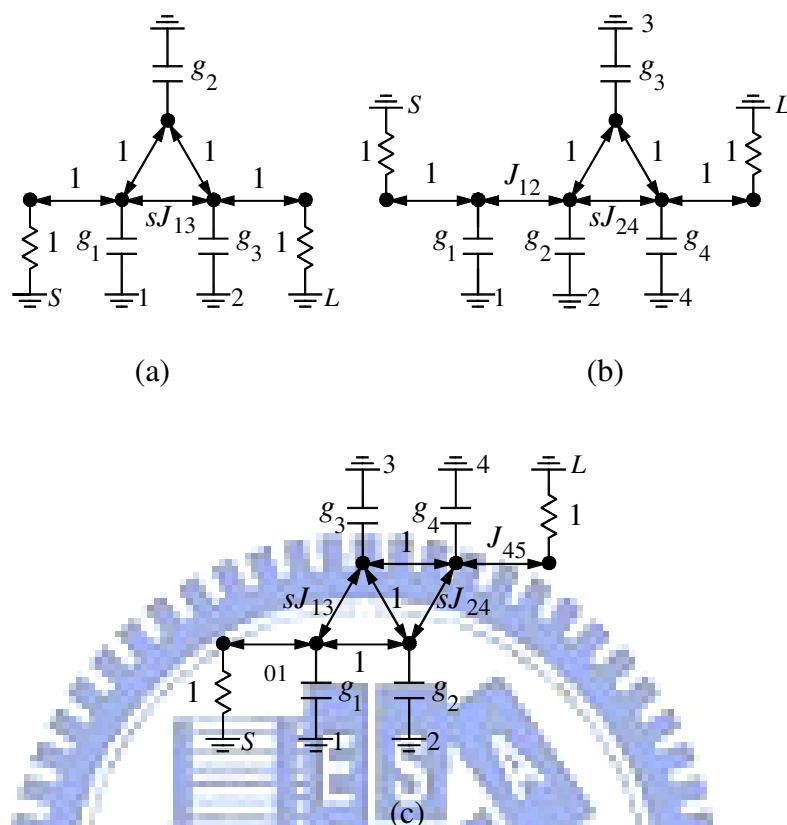
Fig. 3.2 Three possible lowpass prototypes based on trisections. (a) Third-order circuit. (b) Fourth-order circuit with one trisection. (c) Fourth-order circuit with cascade trisections.

$$\begin{bmatrix} 1 & j & 0 & 0 & 0 \\ j & s1.0632 & j & s0.1079 & 0 \\ 0 & j & s1.0298 & j & 0 \\ 0 & s0.1079 & j & s1.0632 & j \\ 0 & 0 & 0 & j & 1 \end{bmatrix} \tag{3.2.4}$$

where source and load nodes are also included. When the sign of J_{12} and J_{23}-inverters is switched to be negative, (3.2.4) becomes

$$\begin{bmatrix} 1 & j & 0 & 0 & 0 \\ j & s1.0632 & -j & s0.1079 & 0 \\ 0 & -j & s1.0298 & -j & 0 \\ 0 & s0.1079 & -j & s1.0632 & j \\ 0 & 0 & 0 & j & 1 \end{bmatrix} \tag{3.2.5}$$

The filter responses will not be changed since (3.1.1) still holds. This means the performance of the filter based on (3.2.5) is the same as (3.2.4). It will be shown later that the change of the sign of a *J*-inverter can be realized by changing the coupling types.

If Ω_z is specified at $s = \pm 1.6$ on the real axis and the in-band ripple is 0.1dB, it can be derived by (2.2.7-10) that the polynomials are $A(s) = D(s) = 2.114s^2 + 1.3797$, $B(s) = 2.0893s$, and $C(s) = 2s^3 + 3.5037s$. When the constant terms of $A(s)$ and $D(s)$ are normalized to unity, we obtain

$$A(s) = D(s) = 1.5322s^2 + 1 \tag{3.2.6}$$

$$B(s) = 1.5143s \tag{3.2.7}$$

$$C(s) = 1.4496s^3 + 2.5396s \tag{3.2.8}$$

The admittance matrix of the network with a pair of real zeros can be expressed as

$$
\begin{bmatrix}
1 & j & 0 & 0 & 0 \\
j & s1.0118 & j & s0.2579 & 0 \\
0 & j & s1.5144 & -j & 0 \\
0 & s0.2579 & -j & s1.0118 & j \\
0 & 0 & 0 & j & 1
\end{bmatrix}
\tag{3.2.9}
$$

Realization of this structure by microstrip resonators will be shown in section 3.3.

The synthesis can be extended to fourth-order prototypes containing one or two trisections, as shown in Fig. 3.2(b) and 3.2(c), respectively. Fig. 3.2(b) shows that a fourth-order network is achieved by cascading a trisection with an additional resonator, the *ABCD* matrix can be derived as

$$A(s) = D(s) = \frac{g_1 g_2 g_3}{J_{12}} s^3 + \frac{g_1 + g_3 J_{12}^2}{J_{12}} s \qquad (3.2.10)$$

$$B(s) = \frac{g_1 g_2 g_3 g_4 - g_1 g_3 J_{24}^2}{J_{12}} s^4 + \left(\frac{g_1 (g_2 + g_4 - 2J_{24})}{J_{12}} + J_{12} g_3 g_4 \right) s^2 + J_{12} \qquad (3.2.11)$$

$$C(s) = \frac{g_2 g_3}{J_{12}} s^2 + \frac{1}{J_{12}} \qquad (3.2.12)$$

In this network, J_{12}-inverter is intentionally used for normalizing the source and load terminations to unity. If Ω_z is specified at $s = \pm j2.3$ and in-band ripple is 0.1 dB, the polynomials has been shown in (2.2.16-18): $A(s) = D(s) = 1.9633s^3 + 2.2588s$, $B(s) = 2.2051s^4 + 4.0108s^2 + 1.1642$, and $C(s) = 1.7482s^2 + 0.85896$. The admittance matrix of the network in Fig. 3.2(b) is obtained as

$$\begin{bmatrix} 1 & j & 0 & 0 & 0 & 0 \\ j & s1.1232 & j1.1642 & 0 & 0 & 0 \\ 0 & j1.1642 & s1.8309 & j & s0.1701 & 0 \\ 0 & 0 & j & s1.1115 & j & 0 \\ 0 & 0 & s0.1701 & j & s1.1390 & j \\ 0 & 0 & 0 & 0 & j & 1 \end{bmatrix} \qquad (3.2.13)$$

It is found that $g_1 \neq g_4$, $g_2 \neq g_3$, and $J_{13} \neq J_{24}$. Thus, the circuit layout of this configuration is not symmetric.

Fig. 3.2(c) shows that the circuit symmetry can be restored if two trisections are arranged in the fourth-order network. If $g_1 = g_4$, $g_2 = g_3$, and $J_{13} = J_{24}$ holds, the *ABCD* matrix can be obtained as

$$A(s) = D(s) = g_1 g_2^2 s^3 + (g_1 + g_2 - 2J_{13})s \tag{3.2.14}$$

$$B(s) = g_1^2 g_2^2 s^4 + g_1(g_1 + 2g_2 - 4J_{13})s^2 + 1 \tag{3.2.15}$$

$$C(s) = g_2^2 s^2 + 1 \tag{3.2.16}$$

It is noted that the J_{01}- and J_{45}-inverter ($J_{45} = J_{01} = 0.9268$) are introduced. The admittance matrix of the network can be derived as

$$
\begin{bmatrix}
1 & j0.9268 & 0 & 0 & 0 & 0 \\
j0.9268 & s0.9647 & j & s0.06787 & 0 & 0 \\
0 & j & s1.4266 & j & s0.06787 & 0 \\
0 & s0.06787 & j & s1.4266 & j & 0 \\
0 & 0 & s0.06787 & j & s0.9647 & j0.9268 \\
0 & 0 & 0 & 0 & j0.9268 & 1
\end{bmatrix}
\tag{3.2.17}
$$

Note that $J_{13} = 0.06787$ in (3.2.17) is smaller in magnitude than $J_{24} = 0.1701$ in (3.2.13) due to the use of two trisections in Fig. 3.2(c). Since the aim of this paper is to design a high-selectivity filter with a reduced number of resonators, only synthesis of networks of order $N \leq 4$ is considered. However, the proposed trisection can be used as a building block in cascade for constructing high-order bandpass filters with plural transmission zeros.

It is known that the admittance matrices in (3.2.9), (3.2.13), and (3.2.17) can be used to obtain the coupling coefficients between adjacent resonators by [1]

$$K_{j,j+1} = \Delta \frac{J_{j,j+1}}{\sqrt{g_j g_{j+1}}} \tag{3.2.18}$$

$$\begin{bmatrix} j\omega C & -j\omega E \\ -j\omega E & j\omega C \end{bmatrix}\begin{bmatrix} V_1 \\ V_2 \end{bmatrix} = \begin{bmatrix} I_{C1} \\ I_{C2} \end{bmatrix}$$

$$\begin{bmatrix} j\omega L & j\omega M \\ j\omega M & j\omega L \end{bmatrix}\begin{bmatrix} I_{L1} \\ I_{L2} \end{bmatrix} = \begin{bmatrix} V_1 \\ V_2 \end{bmatrix}$$
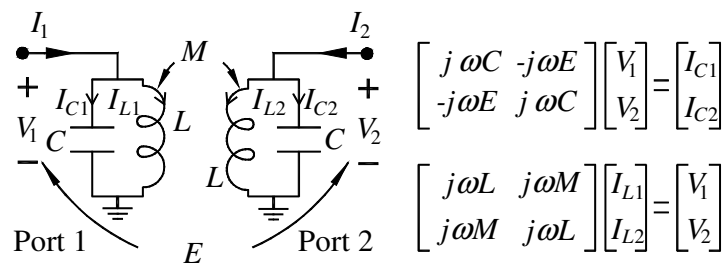
Fig. 3.3.   The equivalent lumped-element circuit of the *J*-inverter for bandpass filters.

where Δ is the fractional bandwidth. For the external Q for the input and output, the expression is as follows [1].

$$(Q_{ext})_i = \frac{g_0 g_1}{\Delta J_{01}^2} \tag{3.2.19a}$$

$$(Q_{ext})_o = \frac{g_N g_{N+1}}{\Delta J_{N,N+1}^2} \tag{3.2.19b}$$

The realization of frequency-dependent coupling will be discussed in the next section.

3.3 Microstrip Frequency-Dependent Admittance Inverter

By the standard lowpass to bandpass transformation, the coupling coefficient between j and $j+2$ resonators can be transformed to

$$K_{j,j+2}\left(\frac{\omega}{\omega_0} - \frac{\omega_0}{\omega}\right) = \frac{J_{j,j+2}}{\sqrt{g_j g_{j+2}}}\left(\frac{\omega}{\omega_0} - \frac{\omega_0}{\omega}\right) \tag{3.3.1}$$

since complex frequency variable s is changed to $j(\omega/\omega_0 - \omega/\omega_0)/\Delta$. This form described by (3.3.1) can be modeled by electric and magnetic coupling between two

coupled resonators as illustrated by the parallel-*LC* network in Fig. 3.3. There are magnetic (*M*) and electric coupling (*E*) between the inductors and capacitors, respectively. From the governing equation described in Fig. 3.3, the *Y*-parameters of the two-port can be derived as follows:

$$Y_{21} = -j\sqrt{\frac{C}{L_r}}\left(\frac{E}{C}\frac{\omega}{\omega_0} - \frac{M}{L}\frac{\omega_0}{\omega}\right) \qquad (3.3.2)$$

$$Y_{11} = j\sqrt{\frac{C}{L_r}}\left(\frac{\omega}{\omega_0} - \frac{\omega_0}{\omega}\right) \qquad (3.3.3)$$

where $\omega_0 = 1/\sqrt{L_r C}$ and $L_r = L(1 - M^2/L^2)$. Comparing of (3.3.1) and (3.3.2) reveals that a *J*-inverter can be realized if $E/C = M/L$ and

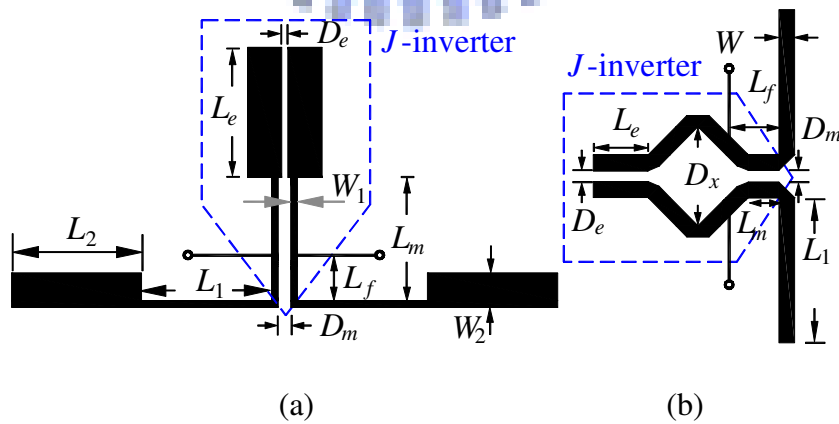$$K_{j,j+2} = \frac{J_{j,j+2}}{\sqrt{g_j g_{j+2}}} = -E/C \qquad (3.3.4)$$

(a)　　　　　　　　　　(b)

Fig. 3.4.　Microstrip frequency-dependent *J*-inverters. (a) Stepped-impedance coupled section. (b) Uniform-impedance coupled section.

In simulation or measurement, the slopes of susceptances $b_{21} = \text{Im}[Y_{21}]/Y_0$ and $b_{11} = \text{Im}[Y_{11}]/Y_0$, i.e., $db_{21}/d\omega$ and $db_{11}/d\omega$ can be used to derive $K_{j,j+2}$ by

$$K_{j,j+2} = -\left(\frac{db_{21}}{d\omega} \bigg/ \frac{db_{11}}{d\omega} \right)\bigg|_{\omega=\omega_0} \tag{3.3.5}$$

where $Y_0 = 1/Z_0$, and Z_0 is port impedance. If b_{11} is not equivalent to b_{22}, (3.3.5) is modified to

$$K_{j,j+2} = -\left(\frac{db_{21}}{d\omega} \bigg/ \sqrt{\left| \frac{db_{11}}{d\omega} \times \frac{db_{22}}{d\omega} \right|} \right)\bigg|_{\omega=\omega_0} \tag{3.3.6}$$

The frequency-dependent J-inverter described by (3.3.1) may not be adequate for the coupling between adjacent resonators on the main signal path since it has a transmission zero at resonance when $\omega = \omega_0$. However, it is useful for non-adjacent coupling to create finite transmission zeros. This frequency-dependent property of electric/magnetic coupling is also found among combline resonators in [43, 44]. However, in the design of combline filter, E or M coupling is intentionally suppressed in order to be independent of frequency since all the non-diagonal elements in the matrix are assumed to a constant.

To realize a frequency-dependent J-inverter for microstrip bandpass filters, the structures in Fig. 3.4 are devised. The E coupling mainly relies on the open ends while the M coupling on the middle section of the resonator. The lengths L_e and L_m and widths D_e and D_m can be determined by fitting the curves of b_{21} and b_{11} of the test circuit to those in (3.3.2). Fig. 3.5 plots the IE3D fullwave simulation results of b_{21} and b_{11} of the circuit in Fig. 5(a) for $D_e = 0.19, 0.23,$ and 0.27 mm. The circuit

has a dielectric constant $\varepsilon_r = 2.2$, thickness $= 0.508$ mm, and port impedance $Z_0 = 50$ Ω. The circuit dimensions are $D_m = 0.79$, $L_1 = 7.79$, $L_2 = L_e = 7.59$, $L_m = 7.19$, $L_f = 1.95$, $W_1 = 0.4$, $W_2 = 2$. From Fig. 3.5(a), it can be obtained that $K_{j,j+2} = 0.102$ for $D_e = 0.27$mm from (3.3.5).
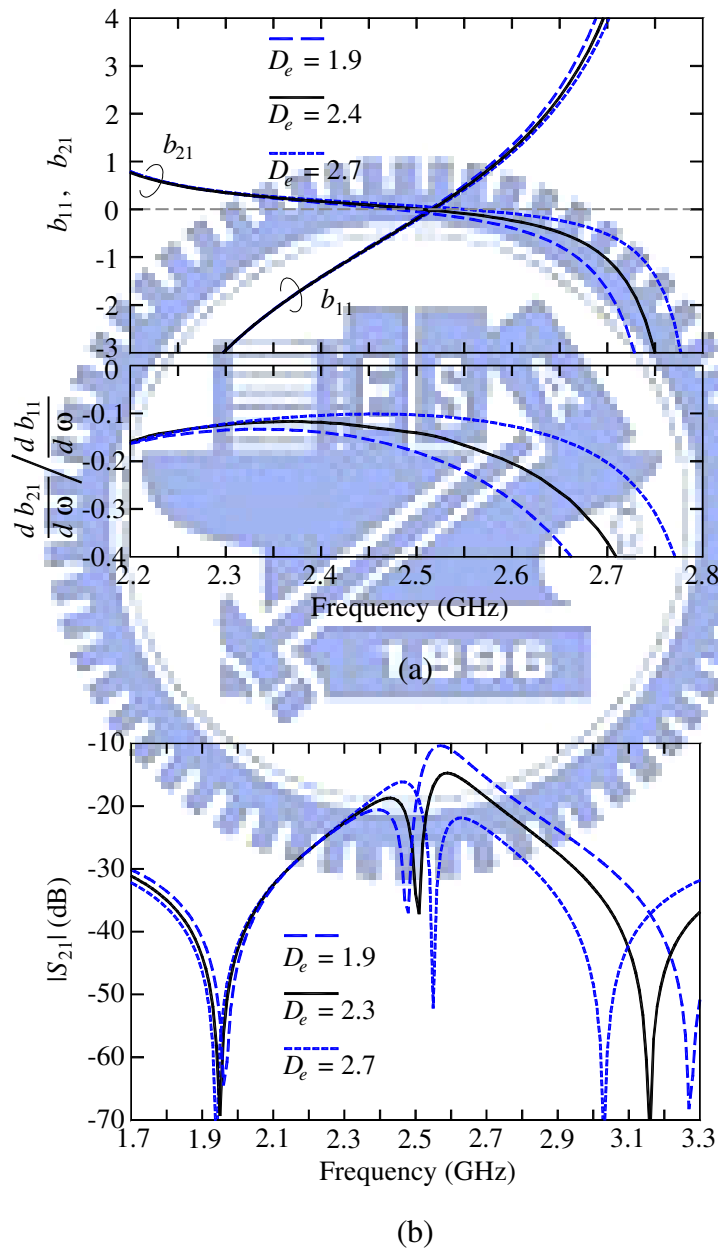

Fig. 3.5. The characteristics of the microstrip *J*-inverter. (a) Normalized *Y*-parameters. (b) $|S_{21}|$ responses.

It is also noted that the value of $|(db_{21}/d\omega)/(db_{11}/d\omega)|$ increases when the operating frequency is away from the center frequency $f_0 = 2.5$ GHz. It is due to the effect of the zeros created by tapped-line input/output, which can be seen from the $|S_{21}|$ responses in Fig. 3.5(b). The consequence is a shift of the zeros toward the center frequency and an increase of the level of the $|S_{21}|$ lobes in stopband. It is noted that the dip of $|S_{21}|$ near 2.5 GHz results from the cancellation of E and M coupling. When the width D_e decreases, Fig. 3.5(a) shows that the value of $|(db_{21}/d\omega)/(db_{11}/d\omega)|$ increases, especially at high frequencies. It implies that the upper zero is more sensitive to the variation of D_e. Fig. 3.5(b) shows the zero caused by tapped-line in upper stopband is also sensitive to this variation.

The coupling structure of Fig. 3.4(b) is similar to that used in narrow-band hairpin-comb filters [40] when the gap width $D_x = 0$. The purpose of D_x is to add a degree of freedom in designing microstrip J-inverters such that the cancellation of E and M coupling can occur at the resonant frequency as required by (3.3.1).

3.4 Simulation and Measurement

3.4.1 Third-order Filters with Four Transmission Zeros

Fig. 3.6 (a) plots the layout of the microstrip trisection filter based on the lowpass prototype of Fig. 3.2(a) with the admittance matrix in (3.2.4). The in-band ripple is 0.1 dB and $\Delta = 6\%$. All experimental circuits are built on a substrate with $\varepsilon_r = 2.2$ and thickness = 0.508 mm. The frequency-dependent microstrip J-inverter is the same as that simulated in section 3.3. The gap D_{12} is determined by the coupling coefficient $K_{12} = 0.0573$ from (3.2.18). The tap point, indicated by L_f, is chosen to match the Q_{si} of a stepped-impedance resonator [34] to $Q_{ext} = 17.72$ from (3.2.19).

Fullwave software package IE3D is used to simulate the circuits before fabrication. The theoretic, simulated, and measured responses are shown in Fig. 3.6(c) and (d). It can be seen that four zeros occur in the stopband. Zeros f_{z1} and f_{z4} are caused by tapped-line while f_{z2} and f_{z3} are by the trisection. When the gap width D_{13} is too large to provide significant E coupling, it is interesting to note that the J_{13}-inverter eventually becomes frequency-independent with only M coupling, which can generate only one zero in lower stopband for this trisection configuration. In measurements, the passband insertion loss is about 1.75 dB, return loss is better than 15dB, and the lobe level in stopband is about -29.5dB. The measured and simulated group delays (τ) are also given. The broadband response shows that the measured 20dB-rejection can be up to 5.75 GHz or 2.3 f_0. It is found that the peak at 6.57 GHz is caused by the first spurious mode of resonator 2, which impedance ratio is slightly lower that of the other resonators and results in lower spurious frequency.

A second realization of the filter is based on (3.2.9), in which the negative J-inverter is implemented by electric coupling. The responses and photo are given in Fig. 3.7. When the gap width D_{13} is too large to provide significant E coupling, the J_{13}-inverter has only M coupling, and hence the circuit has only a zero in the upper stopband.

(a)

(b)

(c)

(d)
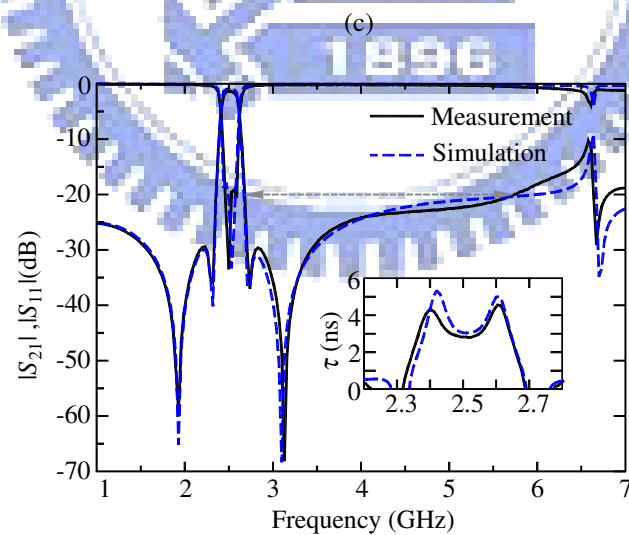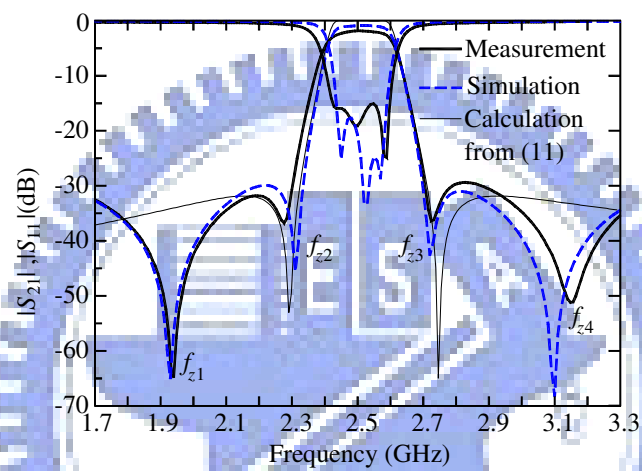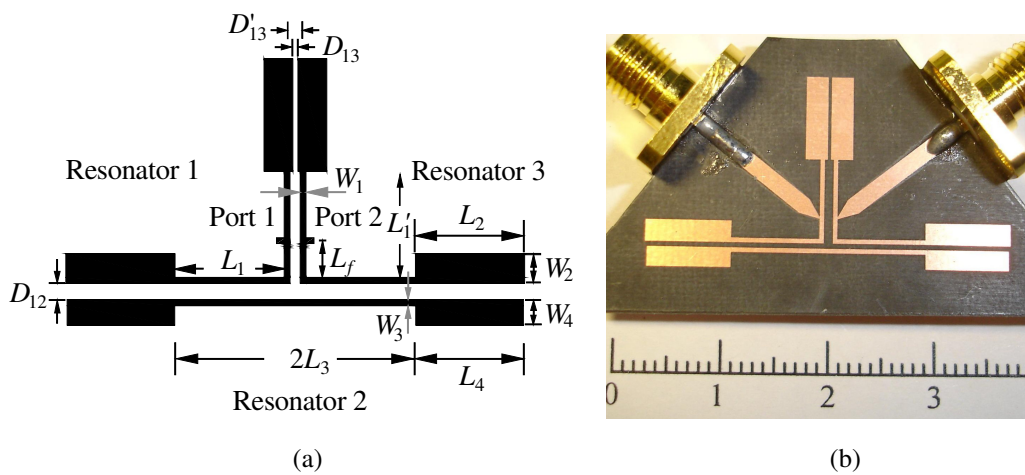
Fig. 3.6. A third-order filter with four zeros. (a) Layout. Dimensions in mm: D_{12} = 0.47, D_{13} = 0.27, D'_{13} = 0.79, L_1 = 7.79, L'_1= 7.19, L_2 = 7.59, L_3 = 8.58, L_4 = 7.42, L_f = 1.95, $W_1 = W_3 = 0.4$, $W_2 = 2$, $W_4 = 1.74$. (b) Photo. (c) $|S_{21}|$ and $|S_{11}|$ responses. (d) Group delay and broadband responses.
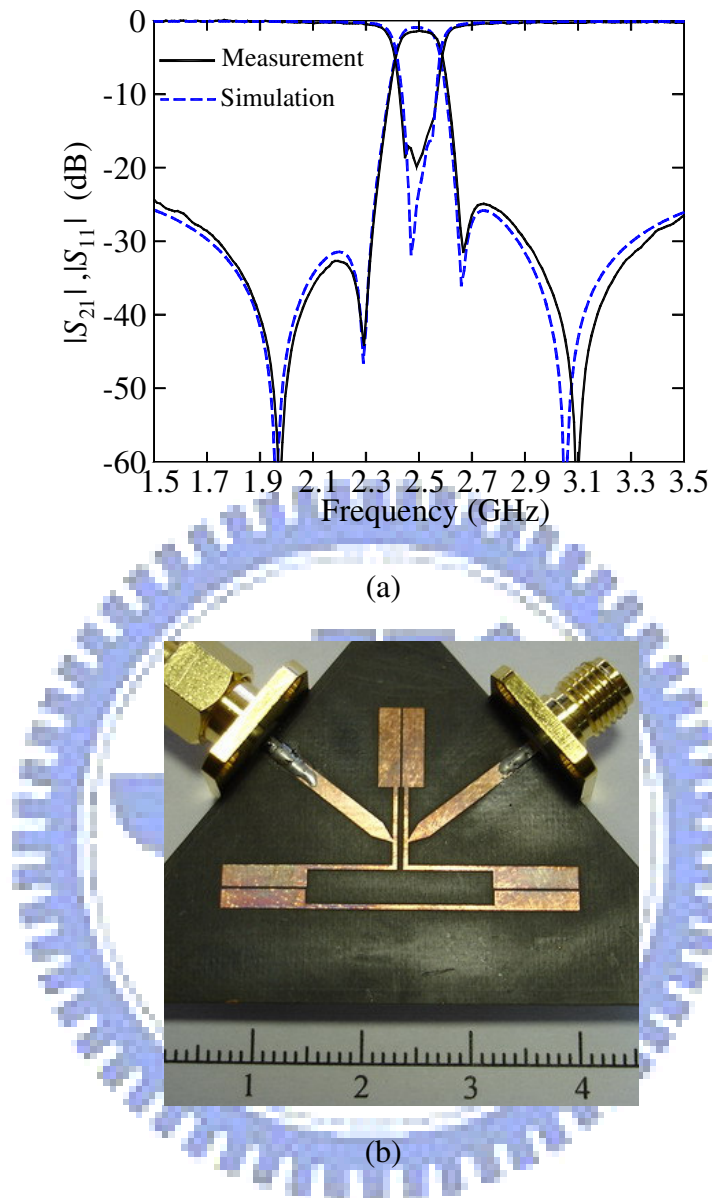
Fig. 3.7. The alternative third-order filter with four zeros. (a) $|S_{21}|$ and $|S_{11}|$ responses. (b) Photo.

3.4.2 Third-order Filters with a Pair of Real Zeros and Two Other Zeros Created by Tapped-Line

This circuit demonstrates the design to create a pair of zeros on the real axis. The zeros are located at $s = \pm 1.6$ and the in-band ripple is 0.1dB. The admittance matrix can be found in (3.2.6). When the fractional bandwidth $\Delta = 5\%$, it can be

obtained the coupling coefficients $K_{12} = -K_{23} = 4.03\%$ and external factors $(Q_{ext})_i = (Q_{ext})_o = 20.38$ from (3.2.18) and (3.2.19), respectively. Fig. 3.8(a) shows that two dips occur at 1.9 and 3.5 GHz in $|S_{21}|$ response, which are caused by tapped input/output. As shown in Fig. 3.8(b), the group-delay response is equalized since a pair of zeros exists on the real axis. From 2.45 to 2.55 GHz, it can be seen that the group delay is within 4.8 and 5.2 ns. Fig. 3.8(c) shows that the broadband results. It is found that the 20-dB rejection level in the upper band can reach to about 8GHz $(3.2f_0)$.

(a)

(b)
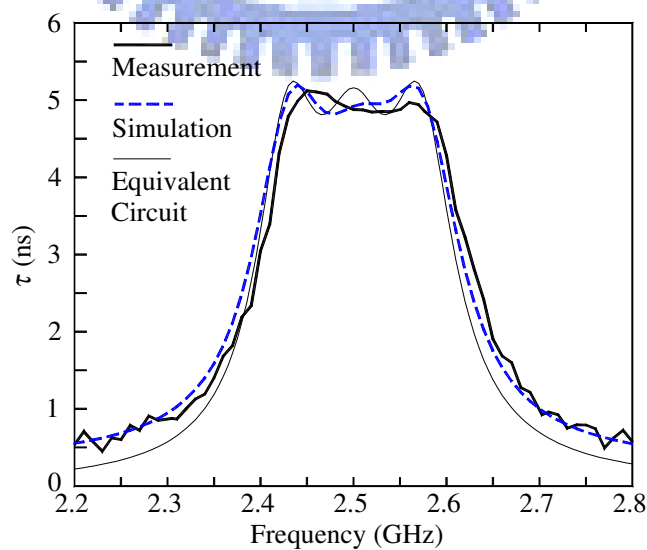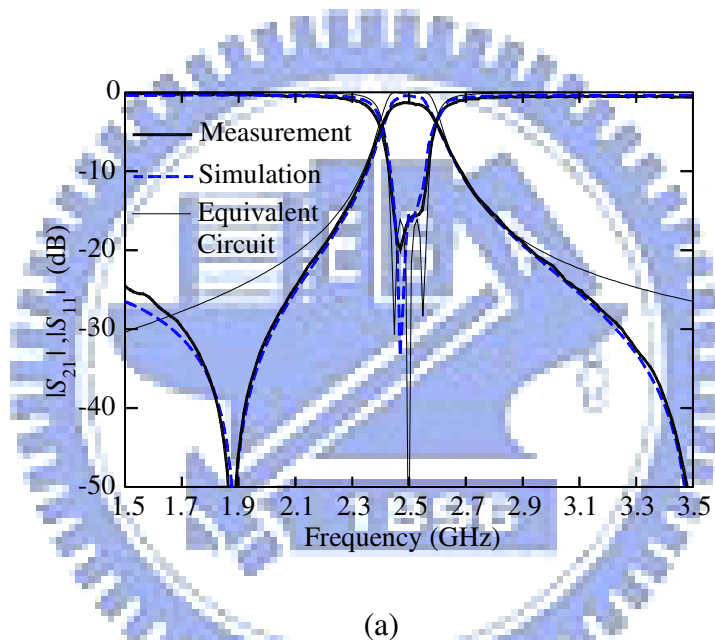
(c)
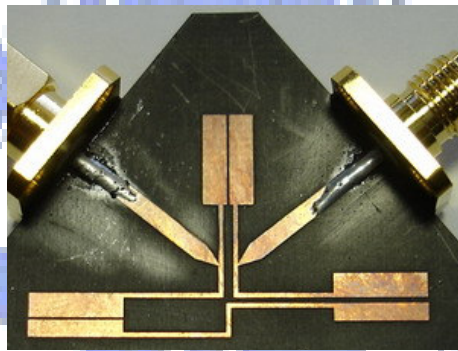
(d)

Fig. 3.8. A third-order filter with two zeros at real frequencies and two others at imaginary frequencies. (a) $|S_{21}|$ and $|S_{11}|$ responses. (b) Group delay (c) Broadband response. (d) Photo.

3.4.3 A Fourth-order Filter with Three Transmission Zeros

This section demonstrates a fourth-order filter based on the prototypes in Fig. 3.2(b) with the admittance matrix in (3.2.13) and uniform-impedance resonators. The J_{24}-inverter can be designed by the method 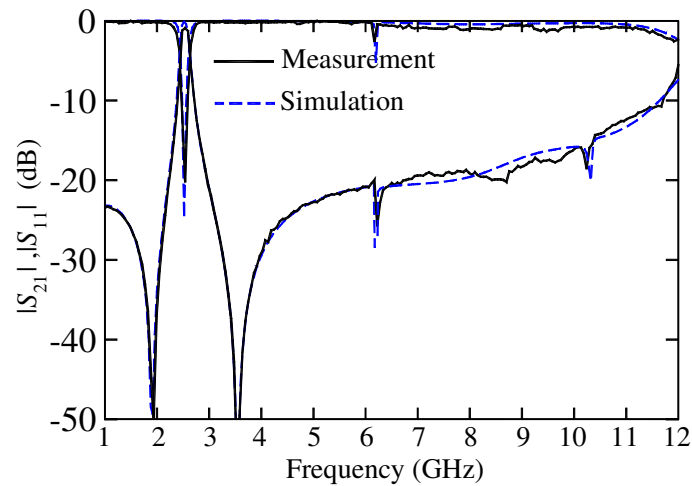developed in section 3.3 except one of the tapped-line in the test circuit is replaced by a coupled feed-line. Equation (3.3.6) is used in calculating $K_{j,j+2}$ since b_{11} is not equivalent to b_{22}. The in-band ripple is 0.1 dB and $\Delta = 5\%$. The layout and filter responses are drawn in Fig. 3.9. It is noted that one arm of resonator 2 is used to implement J_{24}-inverter while the other

arm is used to couple with resonators 1 and 3 by L_{12} and L_{23}, respectively. The frequency of f_{z1} is 0.4 GHz lower than the prediction because the actual values of microstrip J_{24}-inverter at low frequencies are lower than the specified value. In measurements, the passband insertion loss is about 1.96 dB. Due to the first spurious harmonic at $2f_0$, the stopband of a rejection level of 30 dB is only to about 4.62 GHz ($1.85\ f_0$). It can be seen that the zero f_{z3} is determined by the tap point of port 1. There is an alternative tap-point, labeled by T', which has an identical Q_{si} value and can produce a zero in lower stopband. Although this circuit has only three zeros, it can control zero at the frequency f_{z3} by adjusting the length of L_{f1} with a proper width of resonator 1 for matching the port impedance.

(a)

(b)

(c)
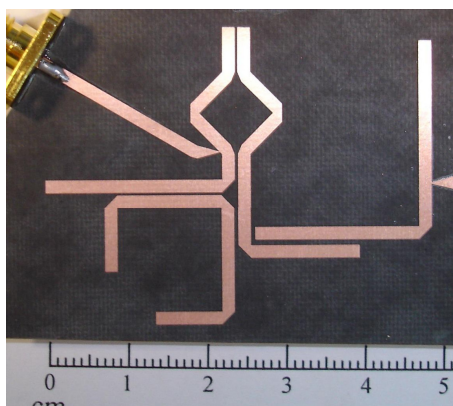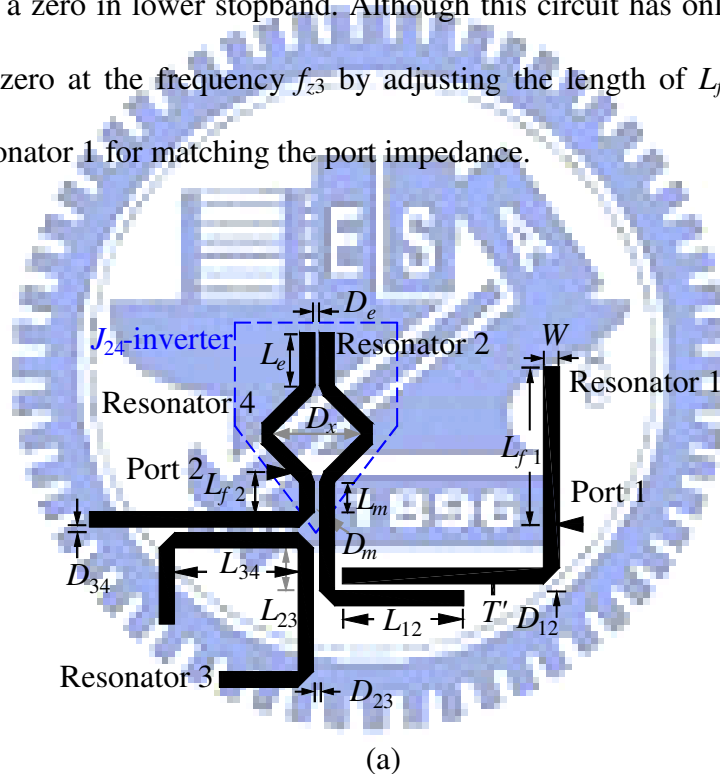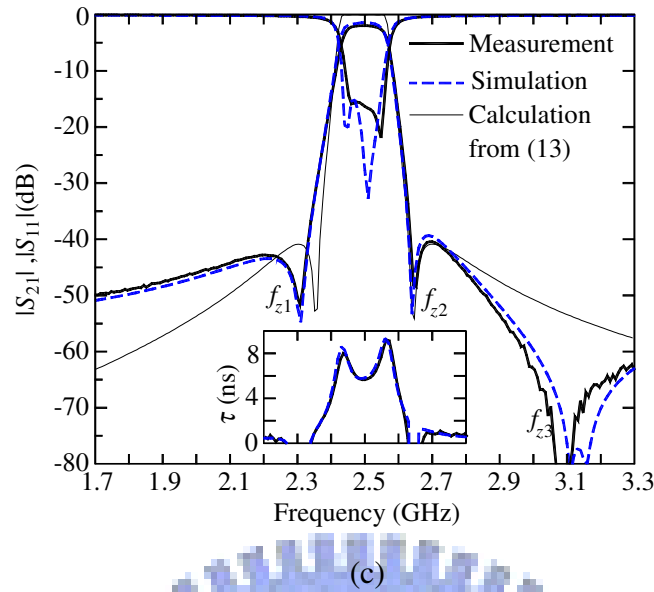
Fig. 3.9. A fourth-order filter with three transmission zeros. (a) Dimensions in mm: $D_{12} = 0.64$, $D_{23} = 0.46$, $D_{34} = 0.3$, $D_e = 0.3$, $D_m = 0.38$, $D_x = 8.94$, $L_{12} = 13.16$, $L_{23} = 4.61$, $L_{34} = 12.6$, $L_e = 5.38$, $L_{f1} = 3.35$, $L_{f2} = 17.12$, $L_m = 3.03$, $W = 1.55$. (b) Photo. (c) Group delay, $|S_{21}|$ and $|S_{11}|$ responses.

3.4.4 A Fourth-order Filter with Five Transmission Zeros

Fig. 3.10 shows the layout and responses of a fourth-order filter based on the prototype in Fig. 3.2(c) with the admittance matrix in (3.2.17) and stepped-impedance resonators. Its in-band ripple and Δ are the same as those in the second example. Note that there are two identical frequency-dependent J-inverters, i.e., J_{13} and J_{24} inverters, in this circuit. For establishing the coupling between resonators 2 and 3, the two trisections have a back-to-back arrangement with a shift by a distance S. This shift can result in the split of the upper zero due to tapped-line, i.e. the zeros at f_{z4} and f_{z5}. The upper rejection band is broadened and a total of five zeros are generated accordingly. In measurement, the insertion loss is 2.34 dB at f_0, 0.38 dB higher than that of the second circuit due to the use of high-impedance line in stepped-impedance resonators. It is found that rejection level of better than 40 dB

can be achieved within the band covering from 2.64 to 4.91 GHz, and the stopband

with a 30dB-rejection level is up to 6.03 GHz ($2.4f_0$). The circuit size is 3.8×3.3 cm^2,

about 55% of the area 5.8×3.9 cm^2 for circuit in section 3.4.3.

(a)

(b)
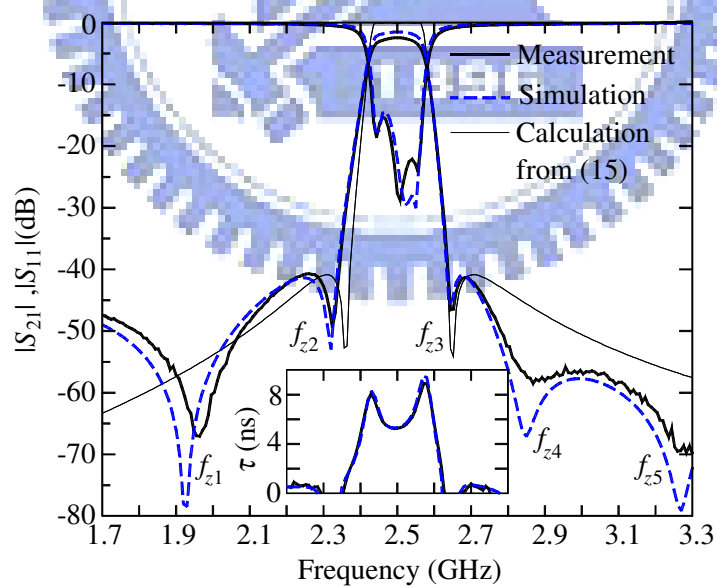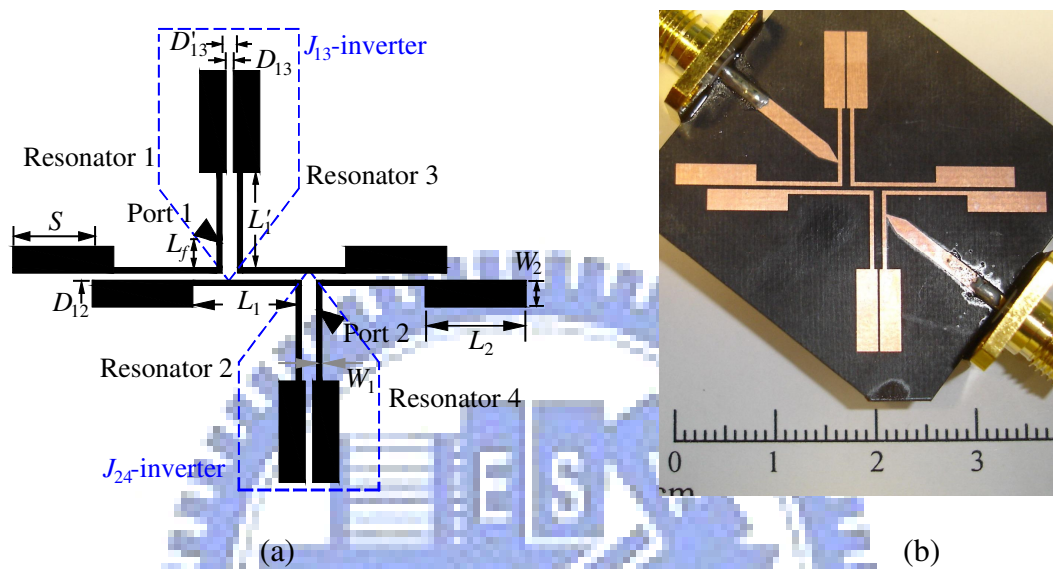
(c)
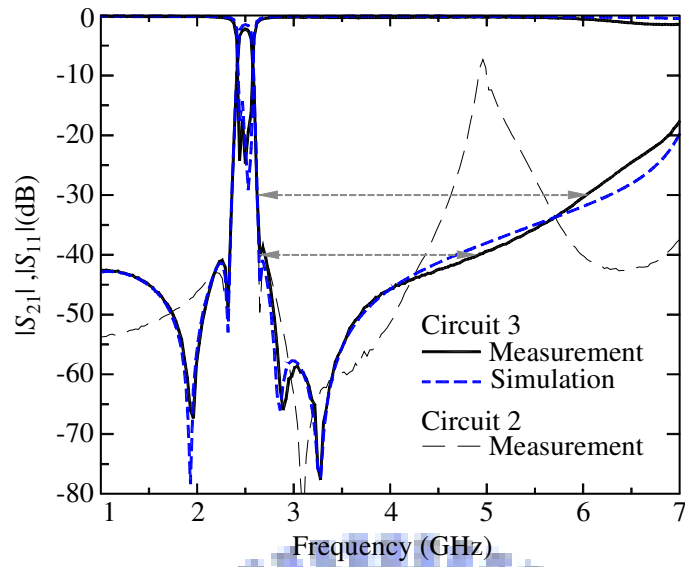
(d)

Fig. 3.10. A fourth-order filter with five zeros. (a) Layout. Dimensions in mm: $D_{12} = 0.4$, $D_{13} = 0.19$, $D'_{13} = 0.79$, $L_1 = 7.79$, $L'_1 = 7.19$, $L_2 = 7.64$, $L_f = 1.95$, $S = 3.0$, $W_1 = 0.4$, $W_2 = 2$. (c) Group delay, $|S_{21}|$ and $|S_{11}|$ responses. (d) Broadband response.

CHAPTER 4

Compact Inline Stepped-Impedance Resonator Filters with a Quasi-Elliptic Function Response

In this chapter, we explore a simple filter structure using the stepped-impedance resonators as building blocks. Fig. 4.1 plots two fourth-order circuits with both symmetric and skew-symmetric feeds. The circuit exhibits several attractive properties, such as compact size, wide upper stopband, elliptic function passband response, and plural transmission zeros. In Fig. 4.1, all resonators form an in-line array so that the circuit occupies a compact area. When order is increased, the circuit size grows only in the direction of the width, which is usually much smaller than the length of the resonator. Although the analysis becomes more complicated, creation of certain transmission zeros in the filter response indeed relies on the nonadjacent coupling. Besides, it is found that the nonadjacent coupling is frequency-dependent. Thus, this filter can be designed by the theory developed in chapter 3.
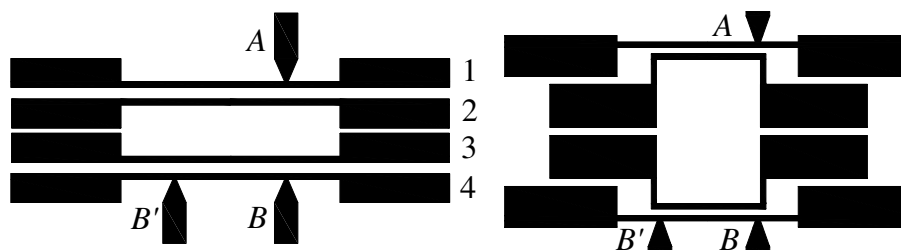
Fig. 4.1. Two in-line fourth-order filters with two tapped input/output schemes: symmetric (A–B) and skew-symmetric (A–B') feeds.
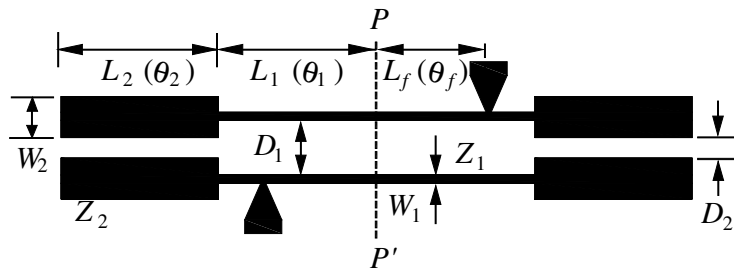
Fig. 4.2.   Generic coupling structure of the in-line bandpass filter.

Here, we limit ourselves to exploring in-line stepped- impedance resonator filters only of orders four, six and eight. Some results for circuits of lower orders can be referred to [46]. The circuit in [46] also possesses a quasi-elliptic function response. Its analysis by the theory of multiple coupled microstrips, however, lacks for design concept for filter synthesis. In the following, Section 4.1 briefly describes the passband synthesis procedure and discusses the coupling properties among the in-line resonators. Section 4.2 explores the existence of the zeros in terms of Y-parameter matrix by taking the adjacent and nonadjacent coupling into account. Section 4.3 addresses the creation of zero by the tapped input/output structure, Section 4.4 presents measured results for three experimental circuits.

4.1 Passband Synthesis

Fig. 4.2 shows the generic basic coupling structure for the filters in Fig. 4.1. Each resonator has one high-Z and two low-Z sections. The former has physical (electric) lengths $2L_1$ ($2\theta_1$) and each of the later has L_2 (θ_2), and their respective widths are W_1 and W_2 with corresponding characteristic impedances Z_1 and Z_2. In addition to D_2, the gap size D_1 can be tuned to establish necessary coupling for synthesizing the passband. Choice of the geometrical dimensions for the resonator

has been extensively studied in [39, 40]. The impedance ratio $R = Z_1/Z_2$ and length ratio $u = \theta_1/(\theta_1 + \theta_2)$ are the key parameters to determine its resonant spectrum. If R and u are properly chosen, the first spurious resonance can be pushed far beyond twice the fundamental frequency or $2f_o$ [40]. For example, if the first higher order resonance occurring at $3f_o$ is desired, $u = 0.5$ and $R = 2.5$ can be used. When $f_o = 2.5$ GHz, geometry parameters can be $L_1 = L_2 = 7.6$ mm, $W_1 = 0.4$ mm and $W_2 = 2.0$ mm for a substrate with $\varepsilon_r = 2.2$ and thickness = 0.508 mm.

Next step is to determine spacing between each pair of adjacent resonators. The coupling coefficient between the jth and $(j + 1)$th resonators, $K_{j,j+1}$, is given by [1]:

$$K_{j,j+1} = \frac{\Delta}{\sqrt{g_j g_{j+1}}} \tag{4.1.1}$$
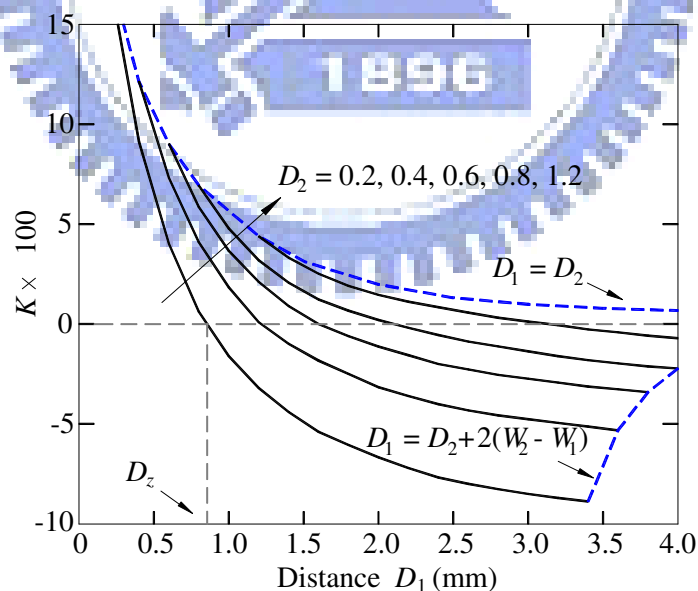
Fig. 4.3.   Coupling coefficients of two stepped-impedance resonators against D_1 for various D_2. $L_1 = L_2 = 7.6$, $W_1 = 0.4$, $W_2 = 2.0$, all in mm. Substrate: $\varepsilon_r = 2.2$, thickness = 0.508 mm.

where g_j is the jth element value of the low-pass filter prototype and Δ the fractional bandwidth. To realize this coefficient for coupled resonators in Fig. 4.2, the test method in [10] can be invoked. Through weak gap feeds to the coupled resonators, the simulated transmission response will present two peaks. If the peaks are at f_a and f_b, the coefficient can be calculated as

$$K_{j,j+1} = \frac{f_b^2 - f_a^2}{f_b^2 + f_a^2} \qquad (4.1.2)$$

For the fourth-order circuits in Fig. 4.1, the coupling matrix is symmetric about its two main diagonals, i.e., $K_{12} = K_{21} = K_{34} = K_{43}$, $K_{13} = K_{31} = K_{24} = K_{42}$, $K_{23} = K_{32}$ and $K_{14} = K_{41}$. Thus, only K_{12}, K_{13} and K_{23} need specifying since all diagonal entries K_{jj} are zero and K_{14} is negligible owing to the relatively large space between resonators 1 and 4.

It can be anticipated that change of D_1 will not significantly alter the first resonance of the resonator, but will change magnitude, and even polarity of the coupling coefficient of two coupled resonators. This property is useful for adjusting the resonator geometry when more than one coupling coefficients have to be simultaneously considered in filter synthesis. An example will be given in section 4.3 for such demonstration. For D_2 (mm) = 0.2 to 1.2, Fig. 4.3 plots coupling coefficients of two resonators against D_1. Except for $D_1 = D_2$, each curve runs from positive to negative values when D_1 is increased up to 4 mm. Generally speaking, the structure consists of both electric and magnetic coupling, called the mixed coupling. When D_1 is small, magnitude of magnetic coupling due to current on the thin sections is larger than that of electric coupling between the low-Z sections at

both ends. When D_1 is increased to be large enough for small D_2, on the other hand, electric coupling becomes dominant. The coefficient calculated by (2) is the net coupling which can be electric ($K < 0$) or magnetic ($K > 0$).

The use of curves in Fig. 4.3 can be demonstrated as follows. Suppose we are designing a fourth-order Chebyshev filter with a 0.1-dB ripple and $\Delta = 8\%$. From (4.1.1), the three interstage coupling coefficients are $K_{12} = K_{34} = 0.06648$ and $K_{23} = 0.05261$. If $D_2 = 0.2$ mm is chosen, we have $-0.089 \leq K \leq 0.15$, and the zero-crossing point is at $D_1 = 0.856$ mm. It is obvious that both electric and magnetic coupling can be used to realize each K value. Thus, there are at least two possible designs: one uses $K_{12} = K_{34} < 0$ and $K_{23} > 0$, and the other uses $K_{12} = K_{34} > 0$ and $K_{23} < 0$. The former and the latter are respectively referred as the M- and E-type filters herein.

For the input and output coupling, the tap positions, i.e., L_f in Fig. 4.2, should be determined by matching the singly loaded Q (Q_{si}) of the tapped resonator with the passband specification. The singly loaded Q (Q_{si}) is defined as

$$Q_{si} = R_L \frac{\omega_0}{2} \frac{dB}{d\omega}\bigg|_{\omega_o} \tag{4.1.3}$$

where R_L is the impedance seen by the resonator looking toward the source, ω_o is the operation frequency, and B is the input susceptance of the resonator seen at the tap point. The derivation of (4.1.3) for a stepped-impedance resonator can be referred to [40]. Both M- and E-type circuits can be designed with the symmetric (A–B) or the skew-symmetric (A–B') feeds [41] with identical Q_{si} values and hence identical passband responses. In the rejection bands, nevertheless, they exhibit quite different

characteristics. Figs. 4.4(a) and 4.4(b) show the simulated $|S_{21}|$ responses of the fourth-order M- and E-type filters, respectively.
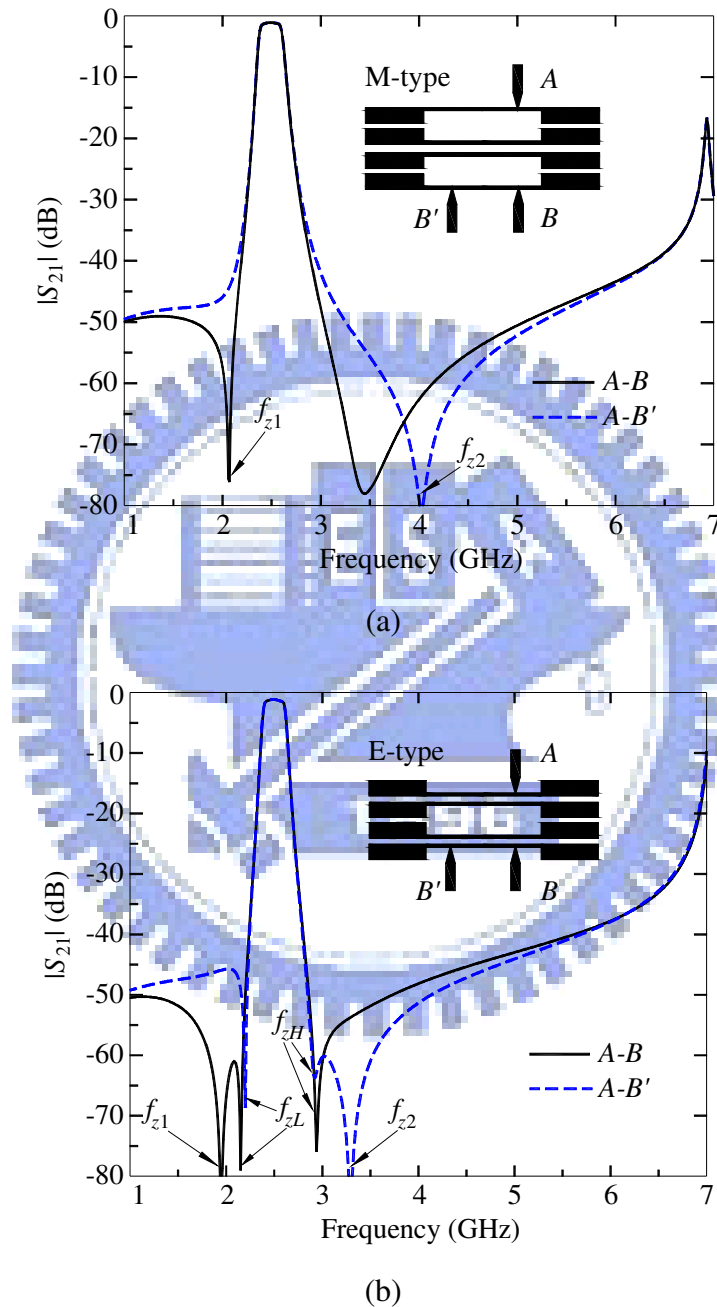

(a)

(b)

Fig. 4.4. Simulation responses of the two fourth-order filters. (a) M-type: $D_{12} = D_{34} = 0.28$, $D_{23} = 1.0$, $L_f = 3.2$. (b) E-type: $D_{12} = D_{34} = 0.82$, $D_{23} = 0.37$, $L_f = 3.2$, all in mm.

The four passbands, say before $|S_{21}| \geq -30$ dB, show very good agreement. In Fig. 4.4(a), both the M-type filters have a transmission zero (f_{z2}) in the upper stopband. The circuit with the symmetric ($A-B$) feed, however, has one more zero (f_{z1}) in the lower stopband. In Fig. 4.4(b), the two E-type filters exhibit sharp transition bands, like those of an elliptic function response, since two zeros, f_{zL} and f_{zH}, are created on both sides of the passband. In addition, there is an extra transmission zero f_{z1} in the lower stopband and f_{z2} in the upper stopband for the ($A-B$) and the ($A-B'$) feeds, respectively. Obviously, the E-type filters possess better frequency selectivity in the stopband than the M-type ones. Thus, the E-type filters are investigated in detail as follows.

4.2 Transmission Zeros Due to Frequency-Dependent Cross Coupling

The occurrence of the zeros in the quadruplet relies on the coupling between the first and the last resonator, which causes two split signals to be out of phase at the output port. In the E-type filters, however, the elliptic function-like response is clearly resulted from a different scheme, since the K_{14} in Fig. 4.1 can be negligible while the nonadjacent coupling coefficients K_{13} and K_{24} should be taken into account. In addition, for predicting the zeros of the particular filter configuration, based on Y-parameter of equivalent circuit of the filter, an analysis method is developed as follows.

The equivalent lumped-circuit model of a filter with two coupled-resonators is shown in Fig. 4.5. Each resonator is modeled with a parallel LC network, and there are magnetic and electric coupling between the inductors and capacitors,

respectively. From the circuit theory, the two-port *Y*-parameters can be derived as follows:

$$Y_{11} = Y_{22} = j\sqrt{\frac{C}{L_r}}\lambda(\omega) \tag{4.2.1}$$

$$Y_{12} = Y_{21} = j\sqrt{\frac{C}{L_r}}\beta(\omega) \tag{4.2.2}$$

where

$$\lambda(\omega) = \frac{\omega}{\omega_0} - \frac{\omega_0}{\omega} \tag{4.2.3}$$

$$\beta(\omega) = \frac{\omega_0}{\omega}m - \frac{\omega}{\omega_0}e \tag{4.2.4}$$

$$\omega_0 = \frac{1}{\sqrt{L_r C}} \tag{4.2.5}$$

$$m = \frac{M}{L} \tag{4.2.6}$$

$$e = \frac{E}{C} \tag{4.2.7}$$
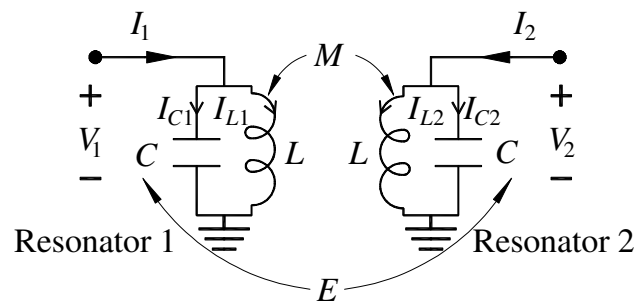
$$L_r = L(1 - m^2) \approx L \tag{4.2.8}$$

Fig. 4.5. The equivalent circuit of two coupled resonators with coupling.

The coefficients m in (4.2.6) and e in (4.2.7) respectively represent magnetic and electric coupling between the two resonators. They are assumed constants over a certain frequency range centered at the design frequency. The natural frequencies f_a and f_b in (4.1.2) of the coupled system can be determined by two conditions: $\lambda(\omega) = \pm\beta(\omega)$, which are obtained by enforcing the determinant of the Y-matrix to zero. It can be validated that

$$K = \frac{f_b^{\,2} - f_a^{\,2}}{f_b^{\,2} + f_a^{\,2}} = \frac{m - e}{1 - em} \approx m - e \qquad (4.2.9)$$

The approximation is valid since $em \ll 1$. The result in (4.2.9) means that the net coupling K calculated by (4.1.2) should be $m - e$. Note that all Y-parameters in (4.2.1) and (4.2.2) are purely imaginary since the circuit is assumed lossless. In (4.2.2), Y_{21} has a zero-crossing point at $\omega = \sqrt{m/e}\,\omega_o$. Thus, its sign over $\omega < \sqrt{m/e}\,\omega_o$ is opposite to that over $\omega > \sqrt{m/e}\,\omega_o$. This property is unusual since in conventional coupling matrix non-diagonal elements are usually assumed independent of frequency. For investigating the possible occurrence of transmission zeros, define the relative phase between Y_{11} and Y_{21} as

$$\theta \equiv \angle Y_{21} - \angle Y_{11} = \angle\left(-\frac{e\dfrac{\omega}{\omega_0} - m\dfrac{\omega_0}{\omega}}{\dfrac{\omega}{\omega_0} - \dfrac{\omega_0}{\omega}} \right) \qquad (4.2.10)$$

It can be deduced from this equation that $\theta = 180^{\circ}$ when $\omega \ll \omega_o$ or $\omega \gg \omega_o$, and $\theta = 0^{\circ}$ when $\omega_o < \omega < \sqrt{m/e}\,\omega_o$ if $m > e$ (i.e., net coupling is magnetic), or $\sqrt{m/e}\,\omega_o < \omega < \omega_o$, if $m < e$ (i.e., net coupling is electric).
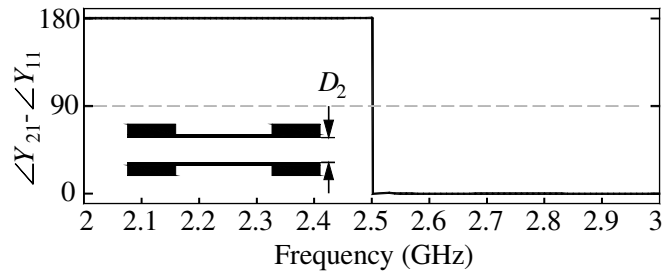
(a)
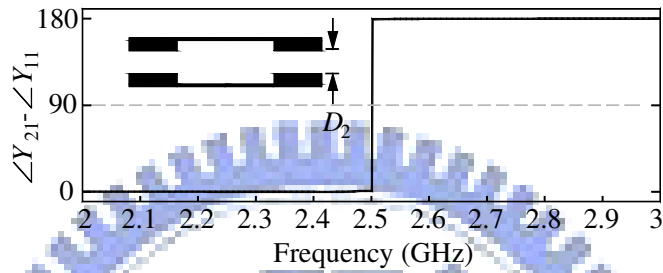
(b)
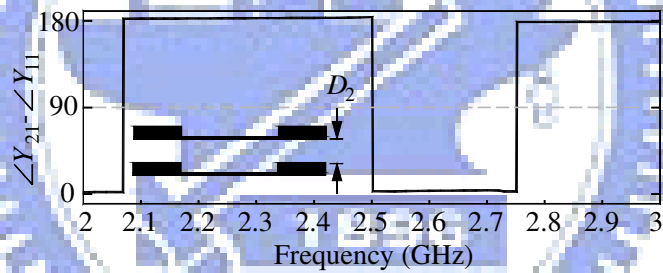
(c)

Fig. 4.6. Responses of $\angle Y_{21} - \angle Y_{11}$ for investigating occurrence of the transmission zeros of the E-type filter in Fig. 4(b). (a) Resonators 1 and 2, $D_2 = 0.82$ mm. (b) Resonators 2 and 3, $D_2 = 0.37$ mm. (c) Resonators 1 and 3, $D_2 = 3.19$ mm.

Fig. 4.6 plots the simulated θ responses for the three basic coupled structures of the E-type filter in Fig. 4.4(b). The Y-parameters are obtained by the software package IE3D. Each θ response shows a jump at $f = f_o$ due to the phase change of the denominator of (4.2.1). Based on Fig. 4.6(a), one can assure that the coupling between resonators 1 and 2 is magnetic- dominant and $K_{12} \approx m \gg e$ for 2 GHz $< f <$

3 GHz. Similarly, the response in Fig. 4.6(b) guarantees $K_{23} \approx e \gg m$. In Fig. 4.6(c) there are extra phase jumps at 2.08 GHz and 2.75 GHz. Two important properties of this coupled structure should be identified by the later jump. First, the type of K_{13} coupling is magnetic, like that is indicated in Fig. 4.6(a). The jump at $f = 2.75$ GHz indicates that Y_{21} changes sign, by (4.2.2), since $\lambda(\omega) > 0$ when $\omega > \omega_o$. Also, by (4.2.2), the m and e values can be extracted since $\sqrt{m/e} = 2.75/2.5 = 1.1$ and $K \approx m - e$ is known by (4.1.2) from simulation data. The jump at 2.08 GHz, however, can not be explained by (4.2.1). It could be due to that the equivalent circuit in Fig. 4.5 has a lower frequency limit for modeling the distributed coupled resonators with a relative large distance in Fig. 4.6(c).

Identifying the type of coupling and value of K_{13} is further investigated for $D_2 = 0.6$ mm and 1.5 mm by Figs. 4.7(a) and 4.7(b), respectively. From Fig. 4.7(a), K_{13} is electric coupling and $\sqrt{m/e} = 2.13/2.5$. Similarly, Fig. 4.6(b) indicates that K_{13} is of the magnetic type and $\sqrt{m/e} = 2.58/2.5$. It is important to identify m and e from the θ responses of coupled resonators in Figs. 4.6(c) and 4.7, since analysis of the transmission zeros relies on it. By analyzing the phase relation of two split signals in the main- and cross-coupled paths, a zero in the upper stopband can occur at $f > 2.75$ GHz. This zero can also be validated by the Y-matrix method given below. Let the filter bandwidth $\Delta = 8\%$ and ripple = 0.1 dB, then the external Q (Q_e) = 13.86. The Y-matrix for the circuit, normalized with respect to $j\sqrt{C/L_r}$, can be expressed as:

$$[Y_n] = \begin{bmatrix} \lambda(\omega) & K_{12} & \beta(\omega) & 0 \\ K_{12} & \lambda(\omega) & -K_{23} & \beta(\omega) \\ \beta(\omega) & -K_{23} & \lambda(\omega) & K_{34} \\ 0 & \beta(\omega) & K_{34} & \lambda(\omega) \end{bmatrix} \qquad (4.2.11)$$
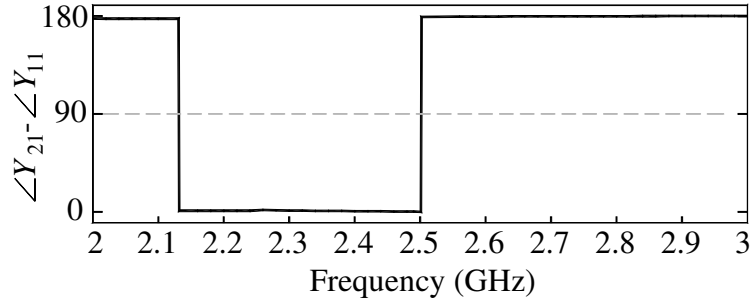
(a)
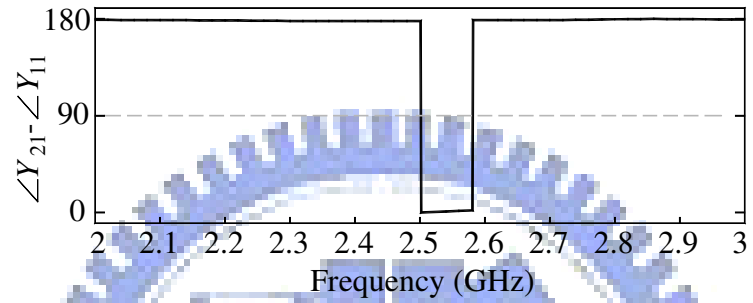
(b)

Fig. 4.7. $\angle Y_{21} - \angle Y_{11}$ responses for identification type of coupling between resonators 1 and 3. (a) $D_2 = 0.6$ mm. (b) $D_2 = 1.5$ mm.

where $K_{12} = K_{34} = 0.06648$ and $K_{23} = 0.05261$. These values are derived from (1). The entries in the first off-diagonal use the following approximation. For example, $Y_{12} \approx K_{12}\omega_0/\omega$ since $K_{12} \approx m \gg e$ and the last term in (4.2.4) is neglected. Values of m and e can be obtained by prescribed zeros at $(1 \pm \xi) \times f_o$. If the two zeros are symmetric about f_o, $m/e \approx 1$ is required. Note that the sign of the elements Y_{13} (Y_{24}) is determined by $\beta(\omega)$. When $\xi = 0.2$ and 0.152, $m = e = 0.012$ and 0.018 can be obtained from the $|S_{21}|$ responses based on (4.2.11), respectively. Fig. 4.8 shows $|S_{21}|$ responses from the matrices with and without the nonadjacent coupling Y_{13} (= Y_{24}). Note that when $m = e = 0$ the response will have no transmission zero. It can be seen from this example that values of m and e can be varied for controlling these two

transmission zeros. One possible way to adjust m and e is to slide or deform the high-Z section of one of the coupled resonators, as shown in Fig. 4.1.

The Y-matrix in (4.2.11) can be easily extended to circuits of order $N = 6$ and 8 with the quasi-elliptic response. The Y-matrix can be established and the frequencies of the zeros can be predicted. For example, the coupling matrices for $N = 6$ are

$$
\begin{bmatrix}
\lambda(\omega) & -K_{12} & \beta(\omega) & 0 & 0 & 0 \\
-K_{12} & \lambda(\omega) & K_{23} & \beta(\omega) & 0 & 0 \\
\beta(\omega) & K_{23} & \lambda(\omega) & -K_{34} & \beta(\omega) & 0 \\
0 & \beta(\omega) & -K_{34} & \lambda(\omega) & K_{45} & \beta(\omega) \\
0 & 0 & \beta(\omega) & K_{45} & \lambda(\omega) & -K_{56} \\
0 & 0 & 0 & \beta(\omega) & -K_{56} & \lambda(\omega)
\end{bmatrix}
\tag{4.2.12}
$$

where $K_{12} = K_{56} = 0.07809$, $K_{23} = K_{45} = 0.05886$, and $K_{34} = 0.05662$, and $m = e = 0.011$. Fig. 4.9 plots the $|S_{21}|$ responses for filters of order $N = 6$ and $N = 8$ with $f_o = 2.5$ GHz, $\Delta = 10\%$ and a 0.1-dB ripple. For all non-adjacent elements $\beta(\omega)$, $m = e = 0.011$ is used.
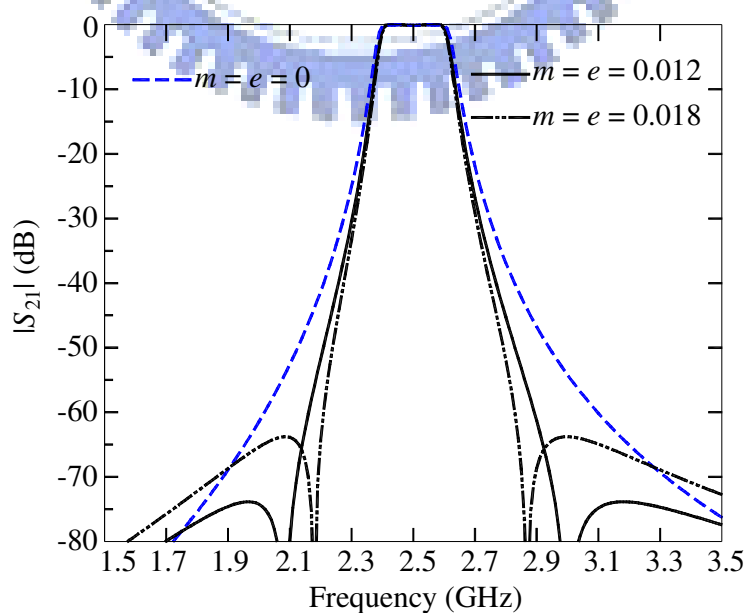
Fig. 4.8. $|S_{21}|$ responses based on coupling matrices in (4.2.11).
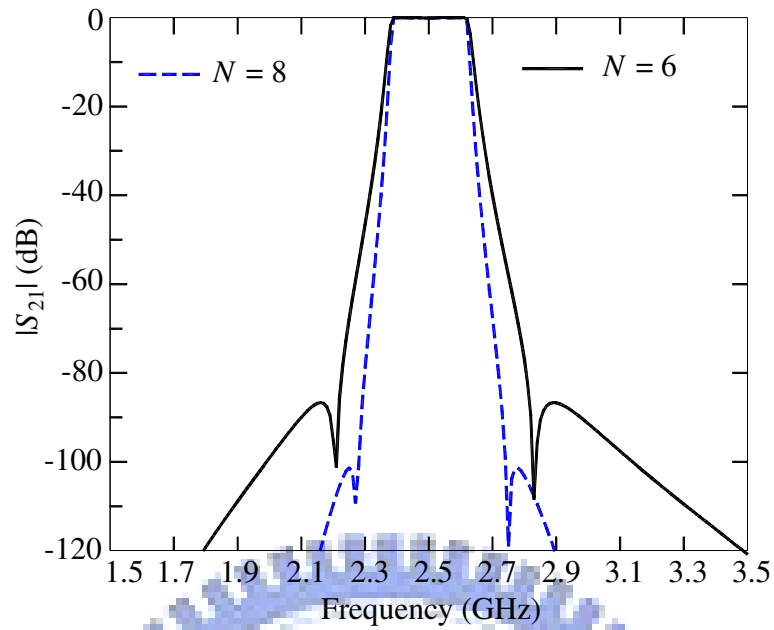
Fig. 4.9. Responses of higher-order in-line filters with $m = e = 0.011$.

4.3 Transmission Zeros due to Tapped Input/Output

Fig. 4.10 plots simulation $|S_{21}|$ responses of the E-type filters with skew-symmetric feed for $L_f = 3.1$, 6 and 9 mm. Impedance transformers are added to keep the Q_{si} value of each tapped resonator unchanged for the three tap positions. It can be seen that frequencies of f_{zL} and f_{zH} as well as the passband do not vary significantly with the changes of L_f. However, the zero f_{z2} moves to higher frequency when tap point is moved away from the center to the edge of the resonator. It reflects the fact that determination of f_{z2} can be dominated by L_f. In the parallel- coupled stepped-impedance resonator filters in [34], a zero can be created at a frequency where the electric length of the arm between the open end of the tapped resonator and the tap point is one quarter wavelength long. The arm used for coupling with adjacent resonator, however, does not create a zero. For the structure in Fig. 4.1, both open ends of the input and output resonators are coupled with their adjacent resonators. Thus, creation of the zero f_{z2} in Fig. 4.10 needs further investigation.

The four-port network in Fig. 4.11(a) is employed for the prediction. Two more

ports are added to the circuit in Fig. 4.1 since in analysis the whole circuit can be

reduced by half due to the symmetry (dash line). Let I_n be total current flowing into

port n, n = 1, 2, 3 or 4. It can be derived that

$$(Z_{21})_{sym} = \frac{1}{2}\left[(Z_{21})_{even} + (Z_{21})_{odd}\right] \tag{4.3.1}$$

where the subscript *sym* represents symmetric feed and *even* and *odd* denote that the

dash line is a magnetic and electric wall, respectively.
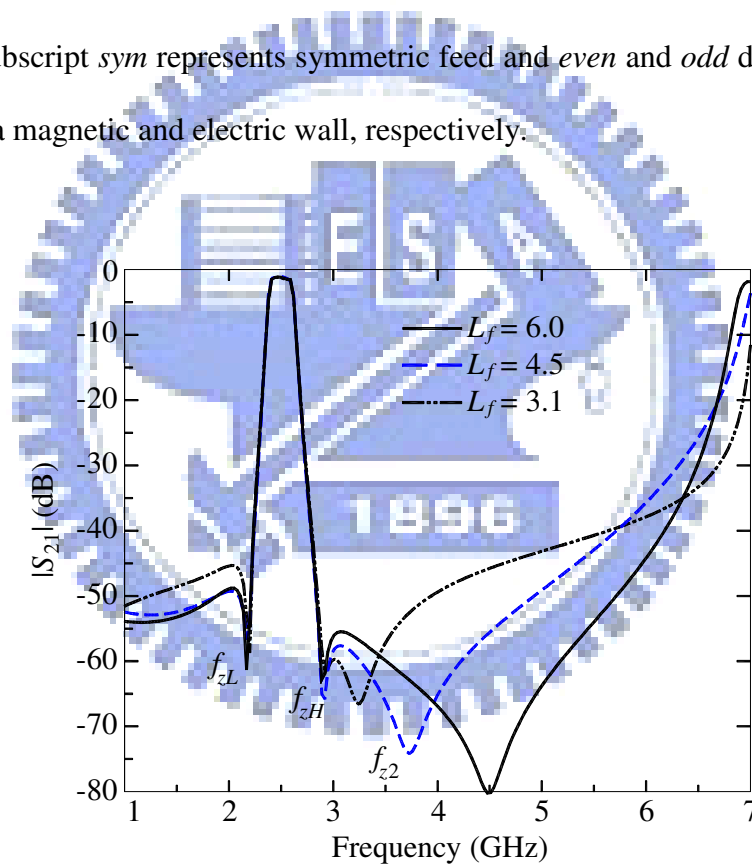
Fig. 4.10. The moves of the tunable transmission zeros due to the slide of tap point
for the E-type filters with skew-symmetric feed.

(a)

(b)
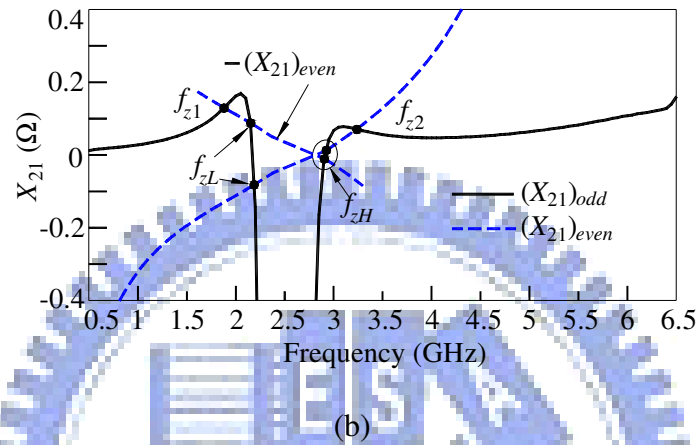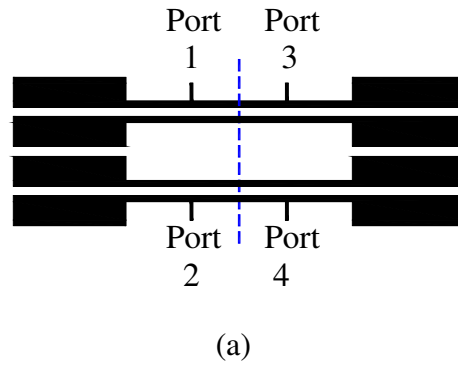
Fig. 4.11 Analysis of f_{z1} and f_{z2}. (a) Four-port network. (b) Responses for X_{21} of the E-type filters. For $-(X_{21})_{even}$, only important part is shown.

(a)

(b)
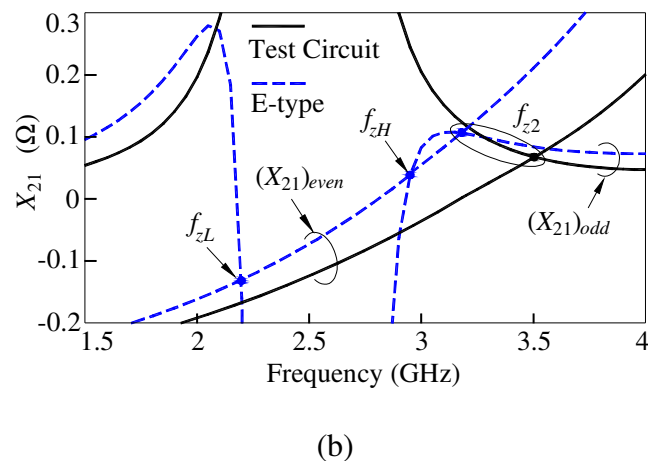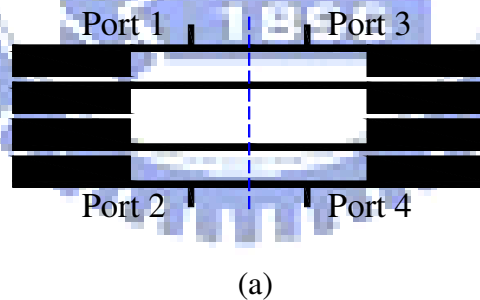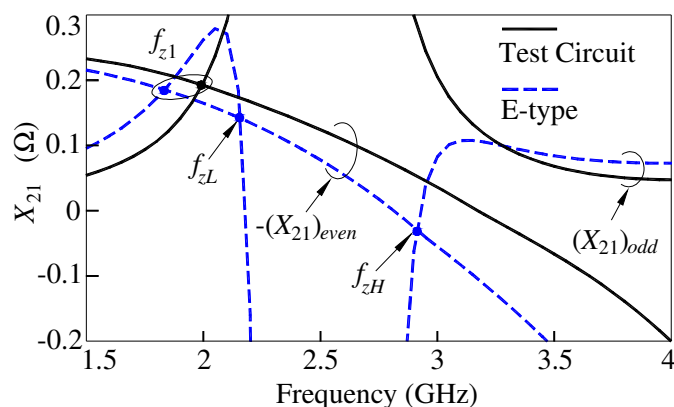
(c)

Fig. 4.12. X_{21} responses for the test circuit and the E-type circuit. (a) Test circuit. (b) Skew-symmetric feed. (c) Symmetric feed.

For the skew-symmetric feed, I_2 and I_3 in Fig. 4.11(a) are set to zero. The transfer impedance Z_{41}, denoted as $(Z_{21})_{skew}$, can be written as

$$(Z_{21})_{skew} = \frac{1}{2}\left[(Z_{21})_{even} - (Z_{21})_{odd}\right]$$ (4.3.2)

For both feeds, zeros of the S_{21} responses can be obtained by enforcing (16) and (17) to zero. The conditions are

$$(Z_{21})_{odd} = \pm(Z_{21})_{even}$$ (4.3.3)

where the plus and minus signs apply to the skew-symmetric and symmetric feeds, respectively. Obviously, complete formulas of $(Z_{21})_{odd}$ and $(Z_{21})_{even}$ will be tedious and complicated since four-microstrip structures are involved [42].

The transfer impedances are purely reactive for lossless structures. Let the reactance be denoted by X and $X_{21} = \mathrm{Im}[Z_{21}]$. Simulated $(X_{21})_{odd}$ and $(X_{21})_{even}$

responses are shown in Fig. 4.11(b), where each intersection point indicates a zero in the $|S_{21}|$ response. Note that the zeros f_{z1} and f_{z2} are in the lower and upper rejection bands for the symmetric and skew-symmetric feeds, respectively. To further investigate the property of the zeros, the behaviour of the circuit in Fig. 4.12 (a) is tested. It is the E-type filter in Fig. 4.4(b) altered by moving the high-Z sections of resonators 1 and 4 outward. Figs. 4.12(b) and 4.12(c) plot the X_{21} responses of the test circuit (solid lines) and the E-type filter (dashed lines). It can be seen that the E-type filter shows three transmission zeros. For the test circuit, however, both f_{zL} and f_{zH} disappear, although f_{z1} and f_{z2} exist respectively for symmetric and skew-symmetric feeds. Based on the results in Figs. 4.12(b) and 4.12(c), $(X_{21})_{odd}$ must be negative or $(Z_{21})_{odd}$ capacitive in the transition bands for creation of f_{zL} and f_{zH} in design of the E-type filters.

(a)   (b)

Fig. 4.13. (a) Group delay and *S*-parameter responses of the E-type filters with symmetric feed. All circuit parameters are in Fig. 4.4(b). (b) Photo.
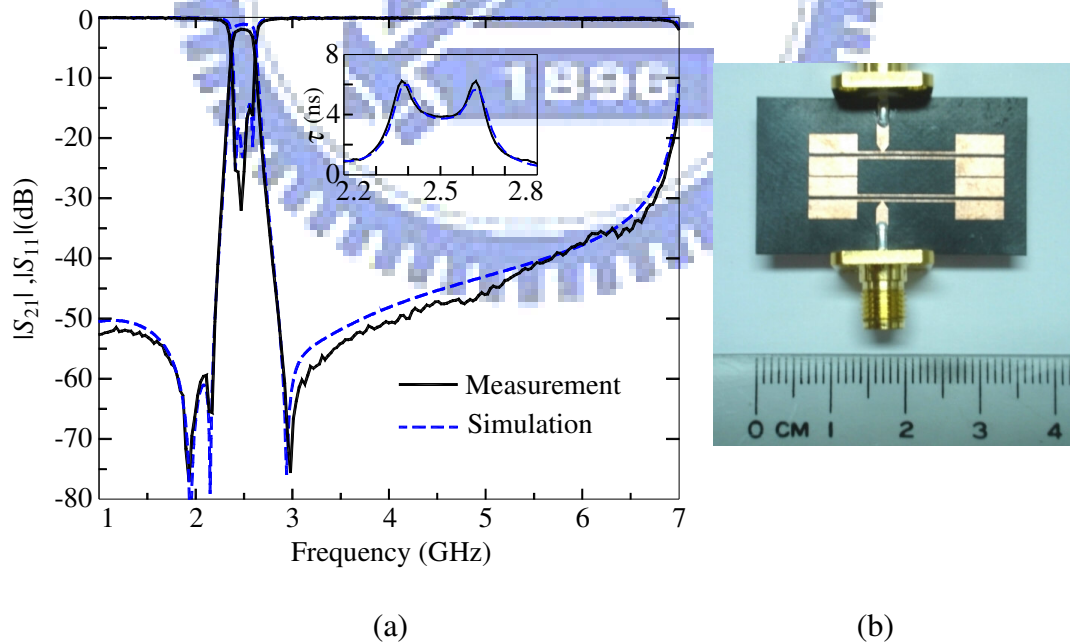
4.4 Simulation and Measurement

Fig. 4.13 plots the simulation and measured responses of the E-type filters with symmetric feed. All geometric parameters are referred to Fig. 4.4(b). The tap points are chosen to match to the Q_{si} value for 50-Ω reference impedance. The measured rejection levels are better than -40 dB up to 5 GHz or $2f_o$. The extra zero f_{z1} is at 1.9 GHz. It is found that rejection levels of better than -60 dB can be achieved within the bands covering from 1.82 to 2.18 GHz and from 2.9 to 3.01GHz. It can be observed that $|S_{21}|$ has a response with sharp transition bands and good symmetry about the center frequency. The measured and simulated group delays (τ) are also given.

The second design demonstrates control of the transmission zeros f_{zL}, f_{zH} and f_{z2}. The center frequency f_o = 2.45GHz and fractional bandwidth Δ = 14% with a 0.1-dB ripple level. Let f_{zL} = 2.05 GHz and f_{zH} = 2.9 GHz, the coupling coefficients K_{12} = 0.1163, K_{23} = 0.0921, m = 0.038 and e = 0.040. The geometric dimensions of the end resonators and the tap position L_f are chosen to locate the zero f_{z2} at $2f_o$ with no transformer. For reducing the circuit size, a substrate with ε_r = 10.2 and thickness = 1.27 mm is used. Fig. 4.14(a) shows the circuit layout with deformed resonators 2 and 3 to simultaneously fulfill required magnitudes of all the coupling coefficients including m and e. To have K_{23} = 0.0921, the high-Z sections of two middle resonators are bent to a U-shape. The distance L_4 can be readily determined by the results shown in Fig. 4.3. At the same time, the low-Z sections are moved inwardly by a distance to simultaneously realize the specified K_{13} and K_{24} values. It could be due to the right-angled bends in the high-Z sections (linewidth = 0.2 mm) that L_2 and L_5 are trimmed by increasing 0.105 mm and 0.425 mm, respectively, for recovering

the resonant frequency shift by the resonator deformation. In the previous example, there is no such problem. The simulated and measured filter responses in Fig. 4.14(b) show good agreement. In measurements, the passband insertion loss is about 2.2 dB and the $|S_{21}|$ notch at 4.9 GHz is about -65 dB. The total circuit size is about 1.5×1.5 cm^2.

(a)

(b)
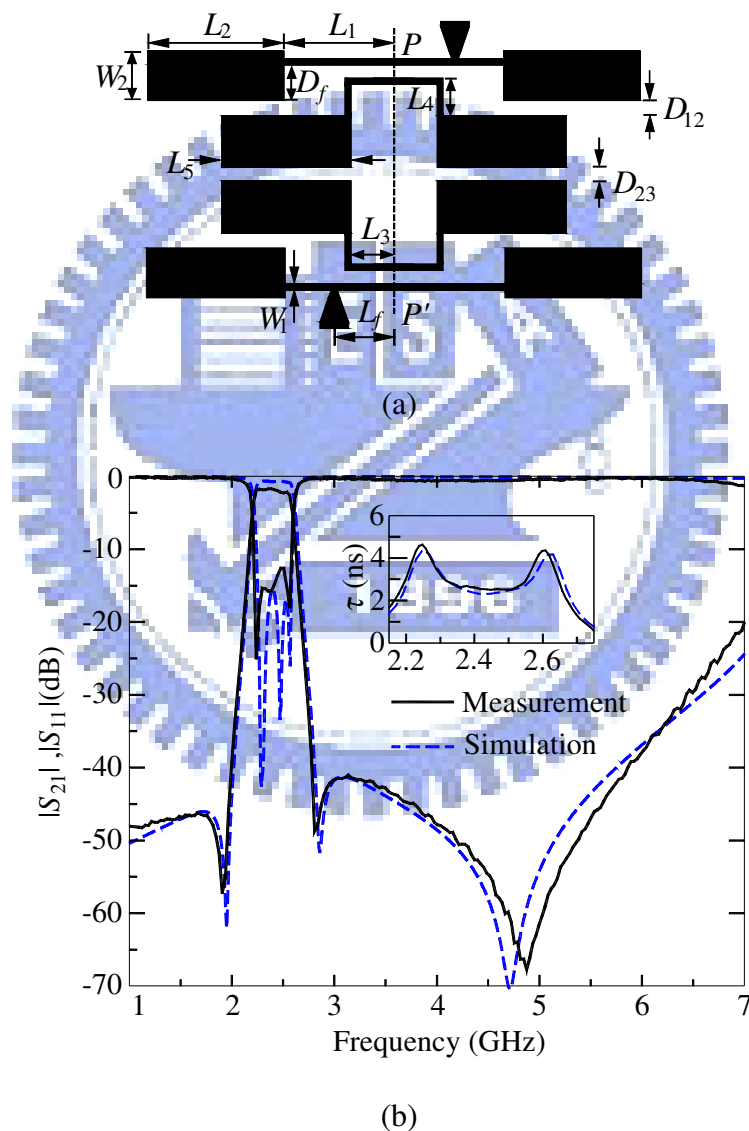
Fig. 4.14. Layout and performances of the E-type filters with skew-symmetric feed. (a) Circuit layout. Dimensions in mm: $L_1 = 3.48$, $L_2 = 3.78$, $L_3 = 2.2$, $L_4 = 1.48$, $L_5 = 4.1$, $L_6 = 1.5$, $L_f = 2.13$, $W_1 = 0.2$, $W_2 = 2.5$, $D_{12} = 0.6$, $D_{23} = 0.5$. (b) Group delay, $|S_{21}|$ and $|S_{11}|$ responses.
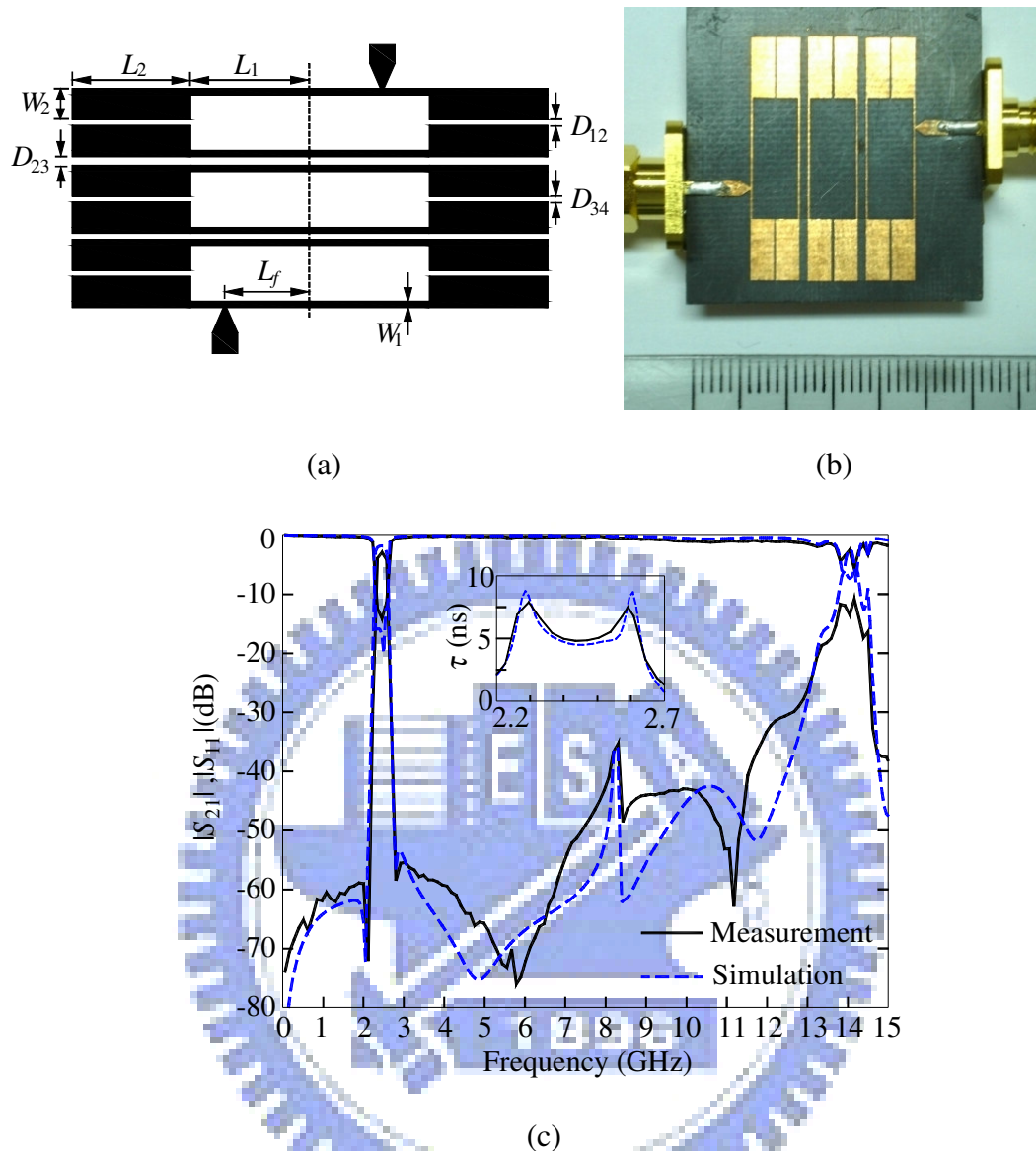
Fig. 4.15. Layout and performances of the sixth-order E-type filters with skew-symmetric feed. (a) Circuit layout. Dimensions in mm: $L_1 = L_2 = 6.32$, $L_f = 3.2$, $W_1 = 0.2$, $W_2 = 2.5$, $D_{12} = D_{56} = 0.14$, $D_{23} = D_{45} = 0.82$, $D_{34} = 0.23$. (b) Photo. (c) Group delay, $|S_{21}|$ and $|S_{11}|$ responses.

The third example is a sixth-order filter built on a substrate with $\varepsilon_r = 2.2$ and thickness = 0.508 mm. The center frequency $f_o = 2.45$ GHz, ripple = 0.1 dB and $\Delta = 10\%$. The resonator geometry is chosen to push the first spurious to $4f_o$. In the filter, the resonators are configured with alternating face-to-face and back-to-back for

establishing all coupling coefficients with proper magnitudes and phases. Note that the coupling coefficients K_{12}, K_{34} and K_{56} are of electric type. Simulation and measured results with skew-symmetric feed are plotted in Fig. 4.15. The insertion loss is 2.5 dB at f_o, inband return loss is better than 15 dB, and the stopband with a rejection level of 50 dB is extended to 7.5 GHz ($3f_o$) and 30 dB to 12.5 GHz ($5f_o$).

CHAPTER 5

Conclusion and Future Work

5.1 Conclusion

Frequency-dependent admittance J-inverter has been proposed to create a pair of transmission zeros in a trisection configuration. Direct synthesis of network elements has been developed for three novel lowpass prototypes by the comparison of polynomial coefficients in $ABCD$ matrices. The elements in the synthesized admittance matrices have been used to determine the coupling coefficients and external Q for experimental bandpass filters. Parallel uniform and stepped-impedance sections have been devised to implement microstrip frequency-dependent J-inverters. It has been shown that tapped-line input/output can be used to generate plural zeros in the proposed configurations. Filters of order $N = 3$ and 4 have been designed to have at most four and five zeros, respectively. For validation, measured results are demonstrated and compared with simulation and theoretic prediction.

Stepped-impedance resonators are arranged in an in-line configuration to make the whole circuit a compact size. The use of the resonators assures a wide upper stopband and the in-line resonator array facilitates new coupling schemes for producing a quasi-elliptic function passband response. Creation of transmission zeros is investigated by Y-matrix parameters of the equivalent circuit of the filter. It is shown that proper non-adjacent elements $Y_{j,j+2}$ are key factors for creating the transmission zeros on both sides of the passband for fourth- and sixth-order filters. Enhanced attenuation rate in transition bands can then be obtained. Formulation of the conditions of the extra zero in rejection bands is also given. It is demonstrated

for the particular in-line structure that the extra zero can be placed in lower and upper stopbands by symmetric and skew-symmetric feeds, respectively. For demonstrations, measured results for three experimental filters are compared with simulation data.

5.2 Future Work

The proposed frequency-dependent coupling structure will be applied to canonical form and cascade structure to design high-order quasi-elliptic function filters with multiple transmission zeros. The study on the filters with multiple frequency-dependent coupling elements will be also investigated. In [47-50], it is seen that many techniques have been proposed to analytically extract the coupling coefficients for a coupled-resonator filter. However, these methods are only suitable for frequency-independent coupling. The extraction technique incorporating frequency-dependent coupling will be developed in the future work.
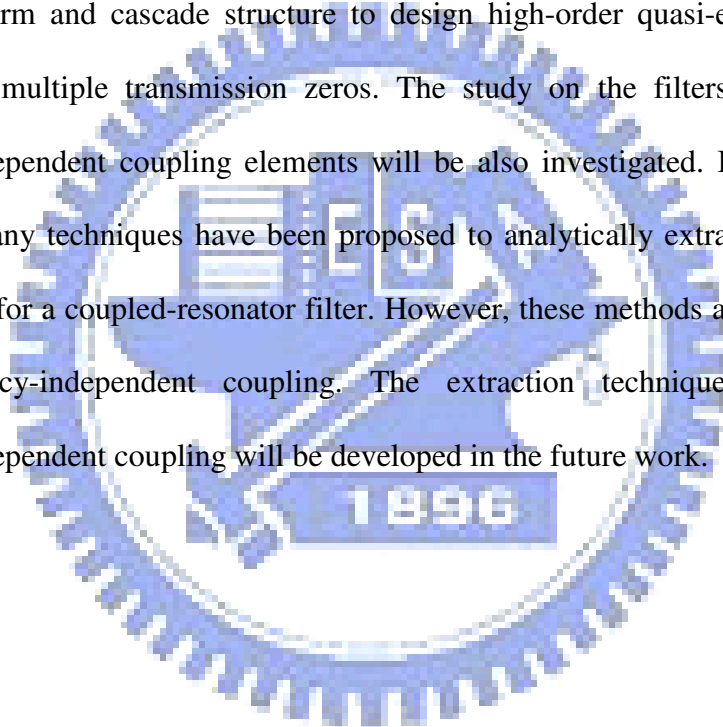
References

[1] G. L. Matthaei, L. Young and E. M. T. Jones, *Microwave Filters, Impedance-Matching Network, and Coupling Structures*. New York: McGraw-Hill, 1964.

[2] R. Levy and S. B. Cohn, "A history of microwave filter research, design, and development," *IEEE Trans. Microw. Theory Tech.*, vol. MTT-32, no. 9, pp. 1055-1067, Sep. 1984.

[3] R. Levy, R. V. Snyder, and G. M. Matthaei, "Design of microwave filters," *IEEE Trans. Microw. Theory Tech.*, vol. 50, no. 3, pp. 783-793, Mar. 2002.

[4] I. C. Hunter, L. B. Billonet, B. Jarry, and P. Guillon, "Microwave filters-applications and technology," *IEEE Trans. Microw. Theory Tech.*, vol. 50, no. 9, pp. 794-805, Mar. 2002.

[5] R. V. Snyder, "Practical aspects of microwave filter development," *IEEE Microw. Mag.*, vol. 8, no. 2, pp. 42-54, Apr. 2007.

[6] D. Swanson and G. Macchiarella, "Microwave filter design by synthesis and optimization," vol. 8, no. 2, pp. 55-69, Apr. 2007.

[7] H. C. Bell, "The coupling matrix in lowpass prototype filters," *IEEE Microw. Mag.*, vol. 8, no. 2, pp. 70-76, Apr. 2007.

[8] F. Seyfert and S. Bila, "General synthesis techniques for coupled resonator networks," *IEEE Microw. Mag.*, vol. 8, no. 5, pp. 98-104, Oct. 2007.

[9] I. C. Hunter, *Theory and Design of Microwave Filters*. Stevenage, U. K.: IEE, 2001.

[10] J.-S. Hong and M. J. Lancaster, *Microstrip Filters for RF/Microwave Applications*, New York: Wiley, 2001.

[11] R. J. Cameron, C. M. Kudsia, and R. R. Mansour, *Microwave Filters for Communication Systems*, New Jersey: Wiley, 2007.

[12] S. B. Cohn, "Direct-coupled-resonator filters," *Proc. IRE*, vol. 45, pp. 187-196, Feb. 1957.

[13] R. M. Kurzrok, "General three-resonator filters in waveguide," *IEEE Trans. Microw. Theory Tech.*, vol. MTT-14, pp. 46-47, Jan. 1966.

[14] R. M. Kurzrok, "General four-resonator filters at microwave frequencies," *IEEE Trans. Microw. Theory Tech.*, vol. MTT-14, pp. 295-296, Jun. 1966.

[15] A. E. Williams, "A four-cavity elliptic waveguide filter," *IEEE Trans. Microw. Theory Tech.*, vol. MTT-18, no. 12, pp. 1109-1114, Dec. 1970.

[16] A. E. Atia and A. E. Williams, "Narrow-bandpass waveguide filters," *IEEE Trans. Microw. Theory Tech.*, vol. MTT-20, no. 4, pp. 258-265, Apr. 1972.

[17] J. D. Rhodes, "A lowpass prototype network for microwave linear phase filters," *IEEE Trans. Microw. Theory Tech.*, vol. MTT-18, no. 6, pp. 290-301, Jun. 1970.

[18] J. D. Rhodes, "The generalized inter-digital linear phase filter," *IEEE Trans. Microw. Theory Tech.*, vol. MTT-18, no. 6, pp. 301-307, Jun. 1970.

[19] J. D. Rhodes, "The generalized direct-coupled cavity linear phase filter," *IEEE Trans. Microw. Theory Tech.*, vol. MTT-18, no. 6, pp. 308-313, Jun. 1970.

[20] H. C. Bell, "Canonical asymmetric coupled-resonator filters," *IEEE Trans. Microw. Theory Tech.*, vol. MTT-30, no. 9, pp. 1335-1340, Sep. 1982.

[21] R. Levy, "Filters with single transmission zeros at real or imaginary frequencies," *IEEE Trans. Microw. Theory Tech.*, vol. MTT-24, no. 4, pp. 172-181, Apr. 1976.

[22] J.-S. Hong and M. J. Lancaster, "Couplings of microstrip square open-loop resonators for cross-coupled planar microwave filters," *IEEE Trans. Microw. Theory Tech.*, vol. 44, no. 11, pp. 2099–2109, Nov. 1996.

[23] J.-S. Hong and M. J. Lancaster, "Design of highly selective microstrip bandpass filters with a single pair of attenuation poles at finite frequencies," *IEEE Trans. Microw. Theory Tech.*, vol. 48, no. 7, pp. 1098–1107, Jul. 2000.

[24] H. C. Bell, "Canonical lowpass prototype network for symmetric coupled-resonator bandpass filters," *Electron. Lett.,* vol. 10, no. 13, pp. 265-266, Jun. 1974.

[25] R. Levy, "Direct synthesis of cascaded quadruple (CQ) filters," *IEEE Trans. Microw. Theory Tech.*, vol. 43, no. 12, pp. 2940-2945, Dec. 1995.

[26] J. D. Rhodes and R. J. Cameron, "General extracted pole synthesis technique with applications to low-loss TE_{011} mode filters," *IEEE Trans. Microw. Theory Tech.*, vol. 28, no. 9, pp. 1018-1028, Sep. 1980.

[27] R. Levy and P. Petre, "Design of CT and CQ filters using approximation and optimization," *IEEE Trans. Microw. Theory Tech.*, vol. 49, no. 12, pp. 2350-2356, Dec. 2001.

[28] C.-C. Yang and C.-Y. Chang, "Microstrip cascade trisection filter," *IEEE Guided Wave Lett*., vol. 9, no. 7, pp. 271-273, Jul. 1999.

[29] U. Rosenberg and W. Hagele, "Advanced multi-mode cavity filter design using source/load-resonance circuit cross couplings." *IEEE Microw. Wireless Compon. Lett*., vol. 2, no. 12, pp. 508-510, Dec. 1992.

[30] I. C. Hunter, J. D. Rhodes, and Vanessa Dassonville, "Dual-mode filters with conductor-loaded dielectric resonators," *IEEE Trans. Microw. Theory Tech.*, vol. 47, no. 12, pp. 2304-2311, Dec. 1999.

[31] S. Amari, "Adaptive synthesis and design of resonator filters with source/load-multiresonator coupling," *IEEE Trans. Microw. Theory Tech.*, vol. 50, no. 8, pp. 1969-1978, Aug. 2002.

[32] S. Amari, "On the maximum number of finite transmission zeros of coupled resonator filters with a given topology," *IEEE Guided Wave Lett*., vol. 9, no. 9, pp. 354-356, Sep. 1999.

[33] S. Amari, "Direct synthesis of folded symmetric resonator filters with source-load coupling," *IEEE Microw. Wireless Compon. Lett*., vol. 11, no. 6, pp. 264-266, Jun. 2001.

[34] C.-K. Liao and C.-Y. Chang, "Design of microstrip quadruplet filters with source-load coupling," *IEEE Trans. Microwave Theory Tech.*, vol. 53, no. 7, pp. 2302–2308, Jul. 2005.

[35] S. Amari and U. Rosenberg, "New building blocks for modular design of elliptic and self-equalized filters," *IEEE Trans. Microw. Theory Tech.*, vol. 52, no. 2, pp. 721–736, Feb. 2004.

[36] C.-K. Liao, P.-L. Chi, and C.-Y. Chang, "Microstrip realization of generalized Chebyshev filters with box-like coupling schemes," *IEEE Trans. Microwave Theory Tech.*, vol. 55, no. 1, pp. 147–153, Jan. 2007.

[37] S. Amari and J. Boremann, "Using frequency-dependent coupling to generate finite attenuation poles in direct-coupled resonator bandpass filters," *IEEE Microw. Wireless Compon. Lett*., vol. 9, no. 10, pp. 404-406, Oct. 1999.

[38] S. Shin and R. V. Snyder, "At least N+1 finite transmission zeros using frequency-variant negative source-load coupling," *IEEE Microw. Wireless Compon. Lett.*, vol. 13, no. 3, pp. 117-119, Mar. 2003.

[39] M. Makimoto and S. Yamashita, "Bandpass filters using parallel coupled stripline stepped impedance resonators," *IEEE Trans. Microw. Theory Tech.*, vol. MTT-28, pp. 1413–1417, Dec. 1980.

[40] J.-T. Kuo and E. Shih, "Microstrip stepped-impedance resonator bandpass filter with an extended optimal rejection bandwidth," *IEEE Trans. Microw. Theory Tech.*, vol. 51, no. 5, pp. 1554–1559, May 2003.

[41] C.-M. Tsai, S.-Y. Lee and C.-C. Tsai, "Performance of a planar filter using a 0° feed structure," *IEEE Trans. Microw. Theory Tech.*, vol. 50, no. 10, pp. 2362–2367, Oct. 2002.

[42] R. J. Cameron, "General coupling matrix synthesis methods for Chebyshev filtering functions," *IEEE Trans. Microw. Theory Tech.*, vol. 47, no. 4, pp. 433-442, Apr. 1999.

[43] R. M. Kurzrok, "Design of combline bandpass filter," *IEEE Trans. Microw. Theory Tech.*, vol. MTT-14, pp. 351–353, Jul. 1966.

[44] H.-W. Yao, K.-A. Zaki, and A. E. Atia, "Full wave modeling of conducting posts in rectangular waveguides and its applications to slot coupled combline filters," *IEEE Trans. Microw. Theory Tech.*, vol. 43, no. 12, pp. 2824–2830, Dec. 1995.

[45] G. L. Matthaei, N. O. Fenzi, R. J. Forse, and S. M. Rohlfing, "Hairpin-comb filters for HTS and other narrow-band applications," *IEEE Trans. Microw. Theory Tech.*, vol. 45, no. 8, pp. 1226–1231, Aug. 1997.

[46] E. Shih and J.-T. Kuo, "A new compact microstrip stacked-SIR bandpass filters with transmission zeros," in *2003 IEEE MTT-S Int. Microwave Symp. Dig.*, Philadelphia, Pennsylvania, Jun. 2003, pp. 1077–1080.

[47] A. Garcia-Lamperez, S. Liorente-Romano, M. Salazar-Palma, and T. K. Sarkar, "Efficient electromagnetic optimization of microwave filters and multiplexers using rational models," *IEEE Trans. Microw. Theory Tech.*, vol. 52, no. 2, pp. 508–521, Feb. 2004.

[48] P. Kozakowski, A. Lamecki, P. Sypek, and M. Mrosowki, "Eigenvalue approach to synthesis of prototype filters with source/load coupling," *IEEE Microw. Wireless Compon. Lett.*, vol. 15, no. 2, pp. 98-100, Feb. 2005.

[49] G. Macchiarella and D. Traina, "A formulation of the Cauchy method suitable for the synthesis of lossless circuit models of microwave filters from lossy measurement, *IEEE Microw. Wireless Compon. Lett.*, vol. 16, no. 5, pp. 243-245, May 2006.

[50] S. Amari and M. Bekheit, "Physical interpretation and implication of similarity transformation in coupled resonator filter design," *IEEE Trans. Microw. Theory Tech.*, vol. 55, no. 6, pp. 1139–1153, Jun. 2007.

博士候選人資料

姓　名　：徐慶陸

性　別　：　男

出生年月日　：　民國　五十六　年　六　月　二十　日

籍　貫　：　　新竹市食品路 41-7 號 4 樓

學　歷　：　　國立交通大學電信工程學系博士班

　　　　　　　（93 年 9 月~）

　　　　　　　國立中山大學電機工程研究所碩士

　　　　　　　（81 年 9 月~83 年 6 月）

　　　　　　　國立交通大學電信工程學系畢業

　　　　　　　（74 年 9 月~78 年 6 月）

經　歷　：　　大華技術學院電子工程系講師

　　　　　　　（88 年 4 月~）

　　　　　　　台揚科技工程師、主任工程師

　　　　　　　（83 年 7 月~88 年 3 月）

論文題目　：具頻率相關耦合之步階阻抗諧振器的準橢圓函數響應

　　　　　　　濾波器之合成與實現

Publication List

A. Journal:

[1]   J.-T. Kuo, **C.-L. Hsu**, and Eric Shih, "Compact planar quasi-elliptic function filter with inline stepped-impedance resonators," *IEEE Microw. Theory Tech.*, vol. 55, no. 8, pp. 1747-1755, Aug. 2007.

[2]   **C.-L. Hsu** and J.-T. Kuo, "A two-stage SIR bandpass filter with an ultra-wide upper rejection band," *IEEE Microw. Wireless Compon. Lett.*, vol. 17, no. 1, pp. 34-36, Jan. 2007.

[3]   **C.-L. Hsu**, J.-T. Kuo, and C.-W. Chang, "Miniaturized dual-band hybrid couplers with respective arbitrary power division ratios," submitted to *IEEE Microw. Theory Tech.*, Jan. 2008.

[4]   **C.-L. Hsu** and J.-T. Kuo, "Trisection bandpass filters with quasi-elliptic function response based on frequency-dependent admittance inverter, submitted to *IEEE Microw. Theory Tech.*, Jul. 2008.

B. Conference:

[1]   **C.-L. Hsu**, C.-H. Yu, and J.-T. Kuo, "Control of transmission zeros by mixed-coupling in a two-stage coupled-resonator filter," *Proc. Asia-Pacific Microw. Conf.*, Dec. 2007, pp. 2369-2372.

[2]   **C.-L. Hsu,** C.-W. Chang, and J.-T. Kuo, "Design of dual-band microstrip rat race coupler with miniaturization," *IEEE MTT-S Int. Microw. Symp. Dig.*, Jun. 2007, pp. 177-180.

[3]   **C.-L. Hsu** and J.-T. Kuo, "Design of microstrip dual-band filters using a double-diplexing configuration," *Proc. Asia-Pacific Microw. Conf.*, Dec. 2006, pp. 1241-1244.

[4]   **C.-L. Hsu** and J.-T. Kuo, "Design of cross-coupled quarter-wave SIR filters with plural transmission zeros," *IEEE MTT-S Int. Microw. Symp. Dig.*, Jun. 2006, pp. 1205-1208.

[5]   **C.-L. Hsu**, J.-T. Kuo, and F.-C. Hsu, "Design of loop resonator filters with a dual-passband response," *Proc. Asia-Pacific Microw. Conf.*, Dec. 2005, pp. 1438-1441.

88

[6]   **C.-L. Hsu**, F.-C. Hsu, and J.-T. Kuo, "Microstrip bandpass filters for ultra-wide (UWB) wireless communication," *IEEE MTT-S Int. Microw. Symp. Dig.*, Jun. 2005, pp. 679-682.